

# On the relationship between ecosystem-scale hyperspectral reflectance and CO<sub>2</sub> exchange in European mountain grasslands

M. Balzarolo<sup>1</sup>, L. Vescovo<sup>2,3</sup>, A. Hammerle<sup>4</sup>, D. Gianelle<sup>2,3</sup>, D. Papale<sup>5</sup>, E. Tomelleri<sup>6</sup>, G. Wohlfahrt<sup>4,6</sup>

[1]{PLECO research group, University of Antwerpen, Wilrijk, Belgium}

[2]{Forests and Biogeochemical Cycles Research Group, Sustainable Agro-Ecosystems and Bioresources Department, Research and Innovation Centre – Fondazione Edmund Mach, S. Michele all'Adige (TN), Italy}

[3]{FoxLaB Research and Innovation Centre - Fondazione Edmund Mach, S. Michele all'Adige (TN), Italy}

[4]{Institute of Ecology, University of Innsbruck, Innsbruck, Austria}

[5]{DIBAF, University of Tuscia, Viterbo, Italy}

[6]{European Academy of Bolzano, Bolzano, Italy}

Correspondence to: M. Balzarolo ([manuela.balzarolo@uantwerpen.be](mailto:manuela.balzarolo@uantwerpen.be))

## Abstract

In this paper we explore the skill of hyperspectral reflectance measurements and vegetation indices (VIs) derived therefrom in estimating carbon dioxide (CO<sub>2</sub>) fluxes (net ecosystem exchange – NEE; gross primary production – GPP), and some key ecophysiological variables related to NEE and GPP (light use efficiency –  $\epsilon$ ; initial quantum yield –  $\alpha$ ; and GPP at saturating light – GPP<sub>max</sub>) of grasslands. Hyperspectral reflectance data (400-1000 nm), CO<sub>2</sub> fluxes and biophysical parameters were measured at three grassland sites located in European mountain regions using standardized protocols. The relationships between CO<sub>2</sub> fluxes, ecophysiological variables and VIs derived using all two-band combinations of wavelengths

1 available from the whole hyperspectral data space were analysed. We found that hyperspectral  
2 VIs generally explained a large fraction of the variability in the investigated dependent variables  
3 and that they generally exhibited more skill in estimating midday and daily average GPP and  
4 NEE, as well as  $GPP_{max}$ , than  $\alpha$  and  $\epsilon$ . Relationships between VIs and  $CO_2$  fluxes and  
5 ecophysiological parameters were site-specific, likely due to differences in soils, vegetation  
6 parameters and environmental conditions. Chlorophyll and water content related VIs (e.g. CI,  
7 NPCI, WI), reflecting seasonal changes in biophysical parameters controlling the photosynthetic  
8 process, explained the largest fraction of variability in most of the dependent variables. **Band  
9 selection based on a combination of a genetic algorithm with random forests (GA-rF) confirmed  
10 that is difficult to select a universal band region suitable for describing ecophysiological  
11 parameters,  $CO_2$  fluxes and biophysical variables across the investigated ecosystems.** Our  
12 findings have major implications for up-scaling terrestrial  $CO_2$  fluxes to larger regions and for  
13 remote and proximal sensing sampling and analysis strategies and call for more cross-site  
14 synthesis studies linking ground-based spectral reflectance with ecosystem-scale  $CO_2$  fluxes.

15

## 16 **1 Introduction**

17 Understanding the mechanisms that drive the carbon dioxide ( $CO_2$ ) exchange of terrestrial  
18 ecosystems is one of the main challenges for ecologists working on climate change (Beer et al.,  
19 2010). Plant gross photosynthesis, also referred to as gross primary productivity (GPP), is one of  
20 the major components of the global carbon cycle. It interacts in complex ways with  
21 environmental factors such as radiation, nutrients, soil moisture, vapor pressure deficit, air  
22 temperature and soil temperature (Drolet et al. 2005). Plant biochemistry and structure determine  
23 many fundamental ecosystem patterns, processes and dynamics (Lambers et al. 1998; Waring  
24 and Running 1998). The canopy nitrogen content regulates the canopy photosynthetic capacity  
25 and the canopy light use efficiency ( $\epsilon$ ) (Ollinger et al., 2008). In addition, the canopy chlorophyll  
26 content plays an important role in controlling ecosystem photosynthesis and carbon gain (Peng et  
27 al., 2011; Gitelson et al., 2006).

28 Optical remote sensing can help ecologists in qualitatively and quantitatively assessing plant and  
29 canopy properties (e.g. biomass (Vescovo et al. 2012), water content (Clevers et al., 2010),  
30 nitrogen content (Ollinger et al., 2008; Knyazikhin et al., 2012), chlorophylls (Gitelson et al.,

1 2006) and photosynthetic rate (Inoue et al., 2008) that drive ecosystem processes related to the  
2 carbon cycle.

3 Empirical and physical based methods have been proposed by several authors to interpret optical  
4 plant and canopy properties. Empirical methods consist of, for example, linear regression  
5 analysis between plant or canopy properties and optical data. The most used empirical methods  
6 are: hyperspectral index methods (Peñuelas et al., 1993; Sims and Gamon, 2002; Inoue et al.,  
7 2008) and multi-variable statistical methods (e.g. stepwise linear regression, genetic algorithm,  
8 neural network (Grossman et al., 1996; Riaño et al., 2005a; Li et al., 2007). Physical methods are  
9 based on the use of radiative transfer models (RTMs) to simulate light absorption and scattering  
10 through the canopy as a function of canopy structure and leaf biochemical composition  
11 (Jacquemoud et al., 2000; Zarco-Tejada et al., 2003). Therefore, RTMs help in quantifying the  
12 contribution of canopy biophysical and biochemical variables to canopy reflectance. One of the  
13 most popular RTM is PROSAIL, based on the coupling of the SAIL canopy bidirectional  
14 reflectance model (Verhoef et al., 1984) and the PROSPECT leaf optical properties model  
15 (Jacquemoud and Baret, 1990). Such models can be used for identifying regions of the light  
16 spectrum that are of particular importance for specific biophysical properties of vegetation. The  
17 sensitivity analysis of the PROSAIL model demonstrated that the red-edge region (between 680  
18 nm to 730 nm) of the spectrum is sensitive to the leaf chlorophyll content and leaf area index  
19 (LAI) (Baret et al., 1992). It is also well accepted that an increase of LAI includes a decrease of  
20 reflectance in the red and an increase in the near-infrared (NIR) region (Jacquemoud, 1993). In  
21 the NIR region, effects of LAI and the leaf angle distribution equally contribute to the reflectance  
22 response (Bacour et al., 2002a). NIR reflectance between 800 nm and 850 nm is also related to  
23 canopy N content (Ollinger et al., 2008; Knyazikhin et al., 2012). In addition, the combination of  
24 the reflectance in NIR and in the short wave infrared region (SWIR) is correlated with canopy  
25 water content (Colombo et al., 2008), but the reflectance between 1000 nm and 1400 nm is also  
26 highly sensitive to LAI. So, some attention is needed when these spectral regions are used to  
27 retrieve water content considering that the canopy properties in a given ecosystem often co-vary  
28 (Bacour et al., 2002b).

29 The drawback of such an approach consists in the fact that the process of building a model  
30 implies approximations and assumptions. For this reason we opted for a purely data based

1 approach such as the hyperspectral index approach. This method consists of the use of spectral  
2 vegetation indices (VIs) defined as spectral band ratios, or normalized band ratios between the  
3 reflectance in the visible (VIS) vs. NIR region or VIS vs. VIS or NIR vs. NIR.

4 The typical optical sampling approach, which is linking spectral observations with CO<sub>2</sub> fluxes, is  
5 based on the Monteith equation (1972, 1977):

$$6 \quad GPP = \varepsilon * PAR * fAPAR \quad (1)$$

7 where  $\varepsilon$  is the light use efficiency and fAPAR is the fraction of absorbed photosynthetically  
8 active radiation); both  $\varepsilon$  and fAPAR can be retrieved by remote optical observations. A wide  
9 number of VIs that can potentially be used to model the productivity of terrestrial ecosystems (as  
10 a proxy of  $\varepsilon$  and fAPAR) has been suggested (Inoue et al., 2008; Coops et al., 2010; Peñuelas et  
11 al., 2011; Rossini et al. 2012). The various VIs differ in their sensitivity to changes in  
12 photosynthetic status. “Greenness indices” – such the widely used Normalized Difference  
13 Vegetation Index (NDVI) – demonstrated to be a good proxy for fAPAR, but are not sensitive to  
14 rapid changes in plant photosynthesis which are induced by common environmental and  
15 anthropogenic stressors (Gitelson et al., 2008; Hmimina et al., 2014; Soudani et al., 2014).  
16 However, in ecosystems characterized by strong dynamics (e.g. grasslands and crops with a  
17 strong green-up and senescence), other VIs are able to effectively monitor seasonal changes in  
18 biophysical parameters controlling canopy photosynthesis such as fAPAR and chlorophyll  
19 content and consequently, can be adopted to monitor the seasonal and spatial variability of  
20 carbon fluxes (Gitelson et al., 2012; Sakowska et al., 2014). Short-term changes in  $\varepsilon$  can be  
21 remotely detected through a spectral proxy of the xanthophyll cycle (Photochemical Reflectance  
22 Index, PRI; Gamon et al., 1992). The PRI is one of the most promising VIs for a direct  
23 estimation of photosynthetic light use efficiency and of its seasonal and diurnal variations  
24 (Nichol et al., 2002). Latest developments of the sun-induced fluorescence method may allow  
25 even more direct remote sensing of plant photosynthesis in the near future (Meroni et al., 2009;  
26 Rossini et al., 2010; Frankenberg et al., 2011). At canopy scale, the relationship between PRI and  
27  $\varepsilon$  was shown to be site-dependent (Garbulsky et al., 2011; Goerner et al., 2011) and strongly  
28 affected by environmental conditions (Soudani et al. 2014).

1 Whereas previous studies have demonstrated the ability of remote sensing data to allow  
2 modelling ecosystem GPP at ecosystem scale (e.g. Gianelle et al., 2009; Wohlfahrt et al., 2010;  
3 Rossini et al. 2012; Sakowska et al., 2014), a universal model for GPP estimation applicable  
4 across different ecosystems and a wide range of environmental conditions is still missing. In  
5 addition, previous studies focussed on single sites with specific characteristics (e.g. climate,  
6 vegetation composition, soil type; see Wohlfahrt et al., 2010) and were often based on the use of  
7 different sensors, platforms and protocols (Balzarolo et al., 2011), making generalisation  
8 difficult. Moreover, most of the studies have either relied on reflectance measurements in a few  
9 spectral wavebands (e.g. Wohlfahrt et al., 2010 and Sakowska et al, 2014) or a minimum number  
10 of bands needed to calculate the most common VIs, missing potentially important information in  
11 under-sampled spectral regions that could help explain carbon fluxes and variability. In order to  
12 overcome such heterogeneity in spectrometry measurements, SpecNet (<http://specnet.info>;  
13 Gamon et al., 2006), the European COST Action ES0903 (EUROSPEC; [http://cost-es0903.fem-  
14 environment.eu/](http://cost-es0903.fem-environment.eu/)) and the COST Action ES1309 (OPTIMISE;  
15 [http://www.cost.eu/domains\\_actions/essem/Actions/ES1309](http://www.cost.eu/domains_actions/essem/Actions/ES1309)) focused on the definition of a  
16 standardized protocol for making optical measurements at the eddy covariance CO<sub>2</sub> flux towers  
17 (Gamon et al., 2010).

18 The overarching objective of the present paper is thus to develop a common framework for  
19 predicting grassland carbon fluxes and ecophysiological parameters based on optical remote  
20 sensing data across measurement sites exposed to diverse natural (climate) and anthropogenic  
21 (management) factors. To this end we combine eddy covariance CO<sub>2</sub> flux measurements with  
22 ground-based hyperspectral reflectance measurements for six different grasslands in Europe. In  
23 order to make the optical and fluxes measurements comparable, these were acquired at the six  
24 sites following a common protocol resulting in a unique standardized data set. We focused on  
25 European grasslands since covering roughly 22% (80 million ha) of the EU-25 land area,  
26 grasslands are among the dominating ecosystem types in Europe (EEA, 2005) and their role in  
27 the European carbon balance has received a lot of scientific interest (Soussana et al., 2007;  
28 Gilmanov et al., 2007; Wohlfahrt et al., 2008; Ciais et al. 2010). While direct measurements of  
29 the carbon exchange have been carried out and are still ongoing at a number of different  
30 grassland sites in Europe –notably in the two EU projects GreenGrass (Soussana et al., 2007) and  
31 CarboMont (Cernusca et al., 2008) – scaling up these plot-level measurements to the continental

1 scale requires a modelling approach, typically based on or supported by remotely sensed data.  
2 Therefore, we believe that this study will improve the current knowledge on modelling the  
3 carbon dynamics of European grasslands.

4

## 5 **2 Materials and methods**

### 6 **2.1 Experimental site description**

7 This study was carried out at six experimental mountain grassland sites in Europe covering  
8 different climatic and grassland management conditions existing in the mountain regions of  
9 Europe, which were already part of the preceding study by Vescovo et al. (2012). This dataset  
10 combined *in-situ* hyperspectral, biophysical and flux measurements based on common protocol  
11 (for more details see sect. 2.2, sect. 2.3 and sect. 2.4). This dataset is unique since no common  
12 protocol for hyperspectral measurements exists in the various eddy covariance networks (e.g.  
13 FLUXNET). In this study, three of these sites (Amplero, Neustift and Monte Bondone, see  
14 Table 1) composed the main dataset used in the analysis, while the other three sites (Table S2 in  
15 Supplemental section) were used to independently validate the models obtained with the main  
16 dataset.

17

18 **Main study sites (Table 1):**

#### 19 *Amplero*

20 The Amplero site is situated in the Mediterranean Appennine mountain region of Italy (41.90409  
21 N, 13.60516 E) at 884 m a.s.l.. This site is characterized by mild, rainy winters and by an intense  
22 drought in summer. Amplero is managed as a hay meadow with one cut in late June and  
23 extensive grazing during summer and autumn.

#### 24 *Monte Bondone*

25 The Monte Bondone site is situated in the Italian Alps (46.01468 N, 11.04583 E) at 1550 m  
26 a.s.l.. This site is characterized by a typical sub-continental climate with mild summers and

1 precipitation peaks in spring and autumn. Monte Bondone is managed as an extensive meadow  
2 with one cut in mid-July.

### 3 *Neustift*

4 The Neustift grassland site is located in the Austrian Alps (47.11620 N, 11.32034 E) at 970 m  
5 a.s.l.. The climate of this area is continental/Alpine, with precipitation peaks during the summer  
6 (July). This site is intensively managed as a hay meadow with three cuts in mid-June, beginning  
7 of August and at the end of September.

8

### 9 *Validation sites:*

#### 10 *Längenfeld*

11 The site Längenfeld is located in the Austrian Alps (47.0612 N, 10.9634 E) at 1180 m a.s.l.. The  
12 climate of this area is continental/Alpine, however compared to the other Alpine sites in this  
13 study, the site receives comparably less precipitation due to rain shadowing effects from both the  
14 North and South. The site is intensively managed as a hay meadow with three cuts in mid-June,  
15 mid-August and mid-October.

16

#### 17 *Leutasch*

18 The site Leutasch is located in the Austrian Alps (47.3780 N, 11.1627 E) at 1115 m a.s.l.. The  
19 climate of this area is Alpine with substantial precipitation due to its position on the north range  
20 of the Alps. The site is extensively managed as a hay meadow with two cuts at the end of June  
21 and beginning of September.

22

#### 23 *Scharnitz*

24 The site Scharnitz is located very close to Leutasch (47.3873 N, 11.2479 E) at 964 m a.s.l. and  
25 the climate is thus very similar to Leutasch. The site is extensively managed as a hay meadow  
26 with two cuts at the beginning of July and beginning of September.

27

## 2.2 Hyperspectral reflectance measurements

The canopy hyperspectral reflectance measurements were collected at each site under clear sky conditions close to solar noon (between 11:00 to 14:00 Central European time) using the same model of a portable spectroradiometer (ASD FieldSpec HandHeld, Inc., Boulder, CO, USA; serial numbers: 1275 for Amplero, 6354 for Monte Bondone in 2006/2013 and 1191 for Neustift, Längenfeld, Leutasch, Scharnitz and Monte Bondone in 2005) at all sites. The spectroradiometer acquires reflectance values between 350 and 1075 nm with a Full Width Half Maximum (FWHM) of 3.5 nm and a spectral resolution of 1 nm. In order to achieve a better match between the eddy covariance flux footprint and optical measurements, a cosine diffuser foreoptic (ASD Remote Cosine Receptor, Inc., Boulder, CO, USA), calibrated by the manufacture, was used for nadir/zenith measurements (Gianelle et al., 2009; Fava et al., 2009; Meroni et al. 2011). The ASD's cosine receptor is designed with a geometry and material that provides a hemispherical field of view (FOV) of 180° and optimizes the cosine response. To reduce the nadir FOV contamination (i.e. sky irradiance and for canopy irradiance) due to the hemispherical view of the sensor the instrument was placed on a 1.5 m long horizontal arm at a height of 1.5 m above the ground. To avoid the zenithal FOV contamination, the measurements were taken at least at a 15 m distance from the eddy covariance tower (maximum height of the tower was 6 m). The vegetation irradiance (sensor pointing nadir) and sky irradiance (sensor pointing zenith) were measured by rotating the spectroradiometer alternately to acquire spectra from the vegetation and from the sky. Hemispherical reflectance was derived as the ratio of reflected to incident radiance. Each reflectance spectrum was automatically calculated and stored by the spectroradiometer as an average of 20 readings. Before starting each spectral sampling, a dark current measurement was done. For more details on experimental set-up see Vescovo et al. (2012). Spectral measurements were collected from spring until the cutting date at Amplero and Monte Bondone, while at the site in Neustift, which is cut three times during the season, spectral measurements were taken about once per week throughout the growing season of 2006.



## 1 **2.3 Biophysical and biochemical canopy properties**

2 Samples for dry phytomass, nitrogen and water content measurements were collected at the time  
3 of the hyperspectral measurements in the field of view of the hyperspectral sensor (see Vescovo  
4 et al. 2012 for more details). A similar dataset was collected in 2013 at Monte Bondone by  
5 combining hyperspectral data with chlorophylls measurements. Chlorophylls samples were  
6 collected in the field of view of the hyperspectral sensor and chlorophylls content was detected  
7 by UV-VI spectroscopy. First, the samples were grinded in presence of liquid nitrogen and then  
8 immersed in 80% acetone solution (0.1 g per 10 ml), shaken for 10 min in an automatic shaker at  
9 250 rpm (Universal Table Shaker 709), and centrifuged at 4000 rpm for 10 min (Eppendorf 5810  
10 R) in order to remove particles from the solution. The absorbance of extracted solutions was  
11 measured at 470, 646.8 and 663.2 nm by a UV/VIS spectrophotometer (Shimadzu UV-1601),  
12 and the concentrations of chlorophyll a ( $C_a$ ), chlorophyll b ( $C_b$ ) and carotenoids ( $C_{x+c}$ ) were  
13 calculated as proposed by Lichtenthaler (1987). The weight of sampled sediment was used to  
14 calculate pigments concentrations per unit leaf mass ( $\text{mg g}^{-1}$ ) and the weight of green biomass  
15 per ground area was used to obtain the total chlorophylls content ( $\text{mg m}^{-2}$ ).

## 16 **2.4 CO<sub>2</sub> flux measurements**

17 Continuous measurements of the net ecosystem CO<sub>2</sub> exchange (NEE) were made by the eddy  
18 covariance (EC) technique (Baldocchi et al., 1996; Aubinet et al., 2012) at the six study sites  
19 using identical instrumentation. The three wind components and the speed of sound were  
20 measured using ultra-sonic anemometers, and CO<sub>2</sub> molar densities using open-path infrared gas  
21 analyzers (IRGAs), as detailed in Tables 1 and S2 in the Supplement section. Raw data were  
22 acquired at 20 Hz and averaged over 30 min time windows in post-processing. Turbulent fluxes  
23 were obtained from raw data by applying block averaging (Monte Bondone, Neustift, validation  
24 sites) or linear de-trending (Amplero) methods with a time window of 30 minutes. A 3D  
25 coordinate correction was performed according to Wilczak et al. (2001). The CO<sub>2</sub> fluxes were  
26 corrected for the effect of air density fluctuations as proposed by Webb et al. (1980). Low- and  
27 high-pass filtering was corrected for following Aubinet et al. (2000) (Amplero, Monte Bondone)  
28 or Moore (1986) (Neustift, validation sites). Data gaps due to sensors malfunctioning or violation  
29 of the assumptions underlying the EC method were removed and filled using the gap-filling and

1 flux-partitioning techniques as proposed in Wohlfahrt et al. (2008). Ecosystem respiration (Reco)  
2 was calculated from the y-intercept of the light response model (see eq. 4). Gross primary  
3 productivity (GPP) was calculated as the difference between NEE and Reco. Half-hourly NEE  
4 and GPP values were averaged between 11:00 to 14:00 solar local time (at the time window of  
5 optical measurements) to allow for direct comparison with the hyperspectral data, and daily sums  
6 were also computed. At each site the following supporting environmental measurements were  
7 acquired: photosynthetically active radiation (PAR; quantum sensors), air temperature (Ta;  
8 PT100, thermistor and thermoelement sensors), and humidity (RH; capacitance sensors) at some  
9 reference height above the canopy, and soil temperature (Ts; PT100, thermistor and  
10 thermoelement sensors) and volumetric water content (SWC; dielectric and time-domain  
11 reflectometry sensors) in the main rooting zone. In this study we used CO<sub>2</sub> flux and  
12 meteorological data of the years 2005 and 2006 for Monte Bondone and of 2006 for the other  
13 sites.

## 14 **2.5 Estimation of grassland ecophysiological parameters**

15 Canopy light use efficiency ( $\epsilon$ ) was derived from photosynthetically active radiation (PAR)  
16 absorbed by the canopy (APAR) as:

$$17 \quad \epsilon = \frac{GPP}{APAR} = \frac{GPP}{PAR * fAPAR} \quad (2)$$

18 and was estimated both at midday and daily time resolution. We estimated the fraction of PAR  
19 absorbed by the canopy (fAPAR) from measured values of the leaf area index (LAI) using the  
20 Lambert-Beer law:

$$21 \quad fAPAR = 0.95 \left( 1 - e^{(-k LAI)} \right) \quad (3)$$

22 where k is the canopy extinction coefficient (fixed at k=0.4 as defined for southern mixed-grass  
23 prairie in Texas; Kiniry et al., 2007) and 0.95 is the proportion of intercepted PAR that is  
24 absorbed by plants (Schwalm et al., 2006). LAI was quantified non-destructively by an indirect  
25 method based on canopy PAR transmission using line PAR sensors (SunScan, Delta-T, UK) and  
26 inversion of a RTM (Wohlfahrt et al., 2001). These measurements were done within the footprint  
27 area of the spectroradiometer simultaneously with the hyperspectral measurements.

1 Three additional key parameters of the response of NEE to PAR were extracted by fitting  
2 measured NEE and PAR to a simple Michaelis-Menten-type model:

$$3 \quad NEE = \frac{-\alpha \text{ PAR} F_{\text{sat}}}{\alpha \text{ PAR} + F_{\text{sat}}} + R_{\text{eco}} \quad (4)$$

4 where  $\alpha$  represents the apparent quantum yield ( $\mu\text{mol CO}_2 \mu\text{mol photons}^{-1}$ ),  $F_{\text{sat}}$  the asymptotic  
5 value of GPP ( $\mu\text{mol CO}_2 \text{ m}^{-2} \text{ s}^{-1}$ ), PAR the photosynthetically active radiation ( $\mu\text{mol photons}$   
6  $\text{m}^{-2} \text{ s}^{-1}$ ) and  $R_{\text{eco}}$  the ecosystem respiration ( $\mu\text{mol CO}_2 \text{ m}^{-2} \text{ s}^{-1}$ ). For all sites, using the  
7 Levenberg-Marquardt (1963) algorithm the parameters of Eq. (4) were estimated by fitting Eq.  
8 (4) to both day and nighttime data, which were pooled into 3-day blocks centered on the date of  
9 the hyperspectral data acquisition. For each acquisition date, we then used Eq. (3) to derive GPP  
10 at an incident PAR of  $1500 \mu\text{mol m}^{-2} \text{ s}^{-1}$ , referred to as  $\text{GPP}_{\text{max}}$  in the following.

## 11 2.6 Hyperspectral data analysis

12 In order to explore the information content of the hyperspectral data for estimating  $\text{CO}_2$  fluxes  
13 (i.e. midday/daily average of NEE and GPP) and ecophysiological parameters (i.e.  $\alpha$ ,  $\varepsilon$  and  
14  $\text{GPP}_{\text{max}}$ ), we performed a correlation analysis between spectral reflectance indices (independent  
15 variables) and these (dependent) variables. To this end, we derived spectral ratio (SR; Eq. (5)),  
16 spectral difference (SD; Eq. (6)) and normalized spectral difference (NSD; Eq. (6)) indices using  
17 all possible two-band (i and j) reflectance ( $\rho$ ) combinations between 400 and 1000 nm (180600  
18 combinations). These three formulations were selected since they represent the most common  
19 equations used to compute vegetation indices (see Table 2).

$$20 \quad SR_{i,j} = \frac{\rho_i}{\rho_j} \quad (5)$$

$$21 \quad SD_{i,j} = \rho_i - \rho_j \quad (6)$$

$$22 \quad NSD_{i,j} = \frac{\rho_i - \rho_j}{\rho_i + \rho_j} \quad (7)$$

23 Linear regression analysis was performed among all possible wavelength-combinations for all  
24 three index-types (SR, NSD and SD) and the investigated dependent variables.

25 The performance of linear models in predicting dependent variables (i.e. carbon fluxes and  
26 ecophysiological parameters) was evaluated by the coefficient of determination ( $R^2$ ) and root

1 mean square error (RMSE). The coefficients of determination ( $R^2$ ) resulting from the linear  
2 models were visualized in correlograms as depicted in an exemplary fashion in Figure 1.

3 We also calculated four SR- and seven NSD-indices which are commonly used in relation to  
4 vegetation activity and  $CO_2$  fluxes (Table 2). Figure 1 shows the location of these indices in the  
5 waveband space of the correlograms. In this analysis, we also considered the Enhanced  
6 Vegetation Index (EVI), which is one of the most frequently used vegetation index to predict  
7  $CO_2$  fluxes. In the Fig. 1 the location of EVI is not shown since this index is computed by the  
8 combination of three spectral bands as shown in Table 2.

9 The robustness of the model selected on the basis of the best band combinations for all  
10 ecophysiological parameters for each site and all sites pooled was tested by the leave-one-out  
11 cross-validation technique. The predictive performance was expressed as the cross-validated  
12 coefficient of determination ( $R^2_{CV}$ ) and the cross-validated root mean square error ( $RMSE_{CV}$ ). In  
13 addition, the capability of the selected models in predicting different ecophysiological  
14 parameters was tested by applying the selected models to the validation dataset (Table S2)  
15 composed by three different grasslands not used in the previous analysis. This dataset was  
16 selected because the hyperspectral and flux data were collected by using exactly the same  
17 protocol applied for the main dataset (see sect.2.1).

18 In order to explore the basis of the correlation between the selected band combinations and  
19 ecophysiological variables (e.g.  $\alpha$ ,  $GPP_{max}$ ,  $GPP$ ,  $\varepsilon$ ) the relationship between the selected bands  
20 and biophysical parameters such as dry phytomass, nitrogen and water content collected during  
21 the field campaign in the same footprint of the hyperspectral measurements was examined.

## 22 **2.7 Band selection based on the combination of random forests and genetic** 23 **algorithm (GA-rF)**

24 In order to complement the more conventional analysis described in the previous section, we also  
25 explored the use of a hybrid feature selection strategy based on a genetic algorithm and random  
26 forests (GA-rF). The first method was used for the feature selection and the second one as  
27 regression for predicting the target variables. First of all, the original dataset was aggregated to  
28 10 nm bands in order to reduce the effects of autocorrelation in frequency space. The algorithm  
29 generates a number of possible model solutions (chromosomes) and uses these to evolve towards

1 an approximation of the best solution of the model. In our case the genes of each chromosome  
2 correspond to the wavebands. We made use of 5 genes for each chromosome in order to  
3 overcome overfitting. Each population of 1000 chromosomes evolved for 200 generations. The  
4 mutation chance was set to the inverse of population size increased by one. The fitness of each  
5 chromosome was measured by applying the random forest algorithm (Breiman, 2001). This was  
6 used as an ensemble method for regression that is based on the uncontrolled development of  
7 decision trees (n=100). We opted for this method because of its demonstrated efficiency with  
8 large datasets. In combining the two methods we choose the mean squared error as the target  
9 variable to be minimized.

10

### 11 **3 Results**

#### 12 **3.1 Seasonal variation of meteorological variables, LAI and CO<sub>2</sub> fluxes**

13 Environmental conditions and the seasonal development of LAI, NEE, GPP  $\alpha$ ,  $\epsilon$  and GPP<sub>max</sub>  
14 during the study period are shown in Figure 2. A strong influence of the typical climatic  
15 conditions at the three study sites is evident: Amplero was characterized by a Mediterranean  
16 climate, with highest incoming radiation and temperatures, and the lowest amount of  
17 precipitation which translated into a substantial seasonal drawdown of soil moisture; Monte  
18 Bondone and Neustift, more influenced by continental Alpine climate, experienced comparably  
19 lower temperatures with higher precipitation and soil moisture with respect to Amplero (Fig. 2).

20 Maximum LAI values were similar at Monte Bondone and Amplero (2.8-3.4 m<sup>2</sup> m<sup>-2</sup>), while,  
21 twice as much leaf area developed at the more intensively managed study site Neustift, which  
22 was also characterized by higher NEE and GPP (i.e. more photosynthesis and net uptake of  
23 CO<sub>2</sub>). The reductions in leaf area associated with the cuts of the grasslands were associated as  
24 expected with marked increases and reductions in NEE and GPP, respectively. The canopy light  
25 use efficiency,  $\epsilon$ , was inversely related to GPP and LAI, peaking at the beginning of the season at  
26 Amplero and Monte Bondone (0.01-0.10  $\mu\text{mol photons } \mu\text{mol CO}_2^{-1}$ ), while for Neustift  $\epsilon$   
27 showed the highest values after the cuts (0.01-0.20  $\mu\text{mol photons } \mu\text{mol CO}_2^{-1}$ ). At  
28 Amplero,  $\alpha$  and GPP<sub>max</sub> peaked in spring and then decreased during the summer drought period,

1 while at Neustift and Monte Bondone, temporal patterns of  $\alpha$  and  $GPP_{max}$  were more strongly  
2 affected by management.

### 3 **3.2 Hyperspectral data and their relation to CO<sub>2</sub> fluxes and ecophysiological** 4 **parameters**

5 Figure 3 reports key spectral signatures of the grasslands collected during the study period. The  
6 reflectances in the NIR region decreased (NIR; 700–1000 nm) and increased in the blue region  
7 (420–540 nm) from early to late spring until the harvest for the Mediterranean grassland of  
8 Amplero (Fig. 3a) (Balzarolo, 2008). This is a typical trend for Mediterranean grasslands  
9 characterized by leaf senescence due to drought conditions (Fava et al., 2007; Vescovo et al.  
10 2012). For Monte Bondone in 2006 and Neustift (Fig. 3b, d) the reflectance in the green (540–  
11 580 nm) and NIR region increased and decreased in the visible region with increasing LAI and  
12 phytomass.

13 Figures 4-6 show correlograms between NSD-, SR- and SD-type indices, respectively, and the  
14 investigated dependent midday ecophysiological parameters and fluxes. The correlograms for  
15 daily data can be found in the Supplement (Figures S1-S3).

16 A number of interesting insights may be gained from Figures 4-6 and Figures S1-S3, which we  
17 summarize in the following:

- 18 (i) The correlograms exhibited quite different patterns – some correlograms showed that a  
19 wide range of band combinations was able to explain the simulated quantities (e.g.  $GPP$  at  
20 Amplero; Fig. 4; Fig. S1), while some correlograms exhibited very pronounced patterns,  
21 with the  $R^2$  value changing greatly with subtle changes in band combinations (e.g.  $\epsilon$  at  
22 Neustift; Fig. 4; Fig. S1).
- 23 (ii) Maximum  $R^2$  values were often clearly higher than the surrounding areas of high  
24 predictive power (e.g.  $\epsilon$  at Amplero; Fig. 4).
- 25 (iii) The different types of indices (compare Figs. 4-6) yielded similarly high correlations with  
26 the same dependent variable at the same site in similar spectral regions, indicating that  
27 band selection is more important for explanatory power than the mathematical formulation  
28 of the VI (i.e. ratio vs. difference, with/without normalization). SR and NSD indices (Figs.  
29 4 and 5) yielded similar results compared to SD indices (Fig. 6).

- 1 (iv) The highest correlations for all dependent variables were found either for indices  
2 combining bands in the visible range (VIS: <700 nm) or the red edge and NIR (NIR: >700  
3 nm), corresponding to spectral regions used by indices such as the SRPI, NPCI, PRI and  
4 NPQI, and the CI and WI, respectively. Spectral regions of well-known indices, such as  
5 NDVI, SR, SIPI or GRI, which exploit the contrasting reflectance magnitudes in the visible  
6 and NIR (Fig. 3), resulted in comparably lower correlations.
- 7 (v) For midday and daily time resolutions different band combinations were selected (e.g.  
8 NEE at Amplero; compare Figs. 5 and S2). For similar selected regions, daily averages  
9 were characterized by higher explanatory power compared to midday averages (e.g.  $\epsilon$  at  
10 Neustift).

11

12 Figure 7 shows the performance of linear regression models for the best NSD-type indices for  
13 midday ecophysiological parameters for each site and all sites pooled (Figure S6 in the  
14 Supplement shows the results of the same analysis for daily averages). Large differences existed  
15 between the study sites in the explanatory power of the same index for the same dependent  
16 variable. The highest  $R^2_{cv}$  and values were generally obtained for Amplero, followed by Neustift  
17 and then Monte Bondone and the lowest  $R^2_{cv}$  values resulted when data from all three sites were  
18 pooled, confirming the difficulties in finding a general relation valid among sites.

19 For Amplero and Neustift the NIR vs. NIR combinations showed a positive linear regression  
20 model with  $\alpha$ ,  $GPP_{max}$  and GPP, while for Monte Bondone a negative linear correlation was  
21 observed. For Amplero the VIS vs. VIS combination showed a good performance in predicting  
22  $\epsilon$ ; the NIR vs. NIR combinations showed good performance for Neustift and VIS vs. NIR  
23 combination for Monte Bondone. The linear models for NEE were site-specific. In fact, Amplero  
24 and Monte Bondone showed a positive linear regression model for NEE but the VIS vs. VIS  
25 band combination was selected for Amplero and NIR vs. NIR combination for Monte Bondone.  
26 Neustift performed well with NEE for NIR vs. NIR combinations, but with an inverse  
27 relationship.

28 The different type of indices (compare Figs. 7, S4 and S5) resulted in similar models. The  
29 different time resolutions gave different models (e.g. GPP,  $\epsilon$  and NEE at Monte Bondone,  
30 compare Figs. 7 and S6 or Figs. S4 and S7 or Figs. S5 and S8).

### 3.3 Correlation between conventional VIs, ecophysiological variables and CO<sub>2</sub> fluxes

The correlation analysis between the conventional VIs, the midday CO<sub>2</sub> fluxes (Table 3) and ecophysiological parameters (Table 4), generally confirmed the results obtained with the hyperspectral data.

For the same dependent variable ( $\alpha$ , GPP<sub>max</sub>, GPP,  $\epsilon$  and NEE), the performance of the various VIs showed large differences between sites. For example, for GPP<sub>max</sub> all of the investigated indices except NPQI resulted in significant linear correlations at Amplero, explaining 41-89% of the variability in GPP<sub>max</sub>. In contrast, only NDVI, PRI, NPCI and SRPI showed a slightly significant linear performance (17-26%) for GPP<sub>max</sub> at Neustift.

The different VIs performed differently in predicting the same dependent variable at the different study sites. For all dependent variables (Tables 3, 4 and S1), the VI resulting in the highest R<sup>2</sup> values was never the same at all sites. Often the best fitting VI at one site resulted in a non-significant correlation at another site. Therefore, none of the dependent variables clearly emerged as the one best predicted (Tables 3, 4 and S1).

When data from all sites were pooled, models showed the same performance for the same VI and dependent variable except for GPP and NEE. The best performing VI for GPP and NEE was SIPI, NPCI performed best for  $\alpha$ , GRI for  $\epsilon$ , SIPI for GPP<sub>max</sub>.

The choice of the averaging period (midday vs. daily) applied to  $\epsilon$ , NEE and GPP did generally not modify the ranking of the VIs, but the R<sup>2</sup> values tended to be similar or somewhat higher at the daily time scale (compare Tables 3 and 4 with Table S1).

### 3.4 Evaluation of the model performance

Figure 8 shows the results of the validation for each ecophysiological parameter and midday averaged fluxes and NSD-, SR- and SD-type indices against data from the validation sites. The models used in the validation are based on the best models determined for each site and by pooling together the two alpine grasslands of Monte Bondone and Neustift. Overall, the results of the validation showed that the models developed were transferable. The best correlation values ( $r > 0.8$ ) were obtained for GPP<sub>max</sub> and GPP for the model developed for Neustift and



1 Monte Bondone. Considering the model based on the Monte Bondone and Neustift sites pooled,  
2 this model performed well with  $\alpha$  for NSD-type index ( $r=0.87$ ). This model also showed good  
3 performance for  $GPP_{max}$  ( $r=0.88$ ),  $GPP$  ( $r=0.92$ ) and  $NEE$  ( $r=0.81$ ) for SD-type indices. Lower  
4 performances were generally found for the models based on the Amplero parameterization. This  
5 is understandable as Monte Bondone and in particular Neustift were structurally and functionally  
6 much more similar to the validation sites compared to Amplero (Tables 1 and S2). Similar  
7 results were obtained for daily averaged  $\epsilon$  and carbon fluxes (Fig. S9 in the Supplement section).

### 8 **3.5 Effect of canopy structure on selected band combinations**

9 Tables 5 and S3 show the results of the correlation analysis between the selected models for  
10 ecophysiological variables and fluxes and biophysical properties of vegetation such as dry  
11 phytomass, nitrogen and water content. Overall, the spectral response in the selected band  
12 combinations for NSD, SR and SD-type indices was strongly related to vegetation properties of  
13 the three grasslands (e.g. nitrogen and dry phytomass) which impacted on their spectral response  
14 in the NIR and VIS regions. For the Mediterranean site (Amplero) and for all eco-physiological  
15 parameters (i.e.  $\alpha$ ,  $GPP_{max}$ ,  $GPP$ ,  $\epsilon$ ), dry phytomass was the main driving factor of the spectral  
16 response in the selected bands, while nitrogen content drove the spectral response in the NIR  
17 region for Neustift. For Monte Bondone, both dry phytomass and nitrogen content affected the  
18 spectral response of the grassland. Similar results were obtained for SR- and SD-type indices.

19 Figs. 9 and S10 in the Supplement show the correlation analysis between the selected bands for  
20 NSD-, SR- and SD-type indices and chlorophylls content for Monte Bondone in 2013. The  
21 chlorophylls content showed a very good correlation for all selected models and for all indices.  
22 The values of  $R^2$  were always higher than the values of  $R^2$  obtained for the other biophysical  
23 variables (Tables 5 and S3). In Figure 9, it is possible to see that, NSD- and SR-type indices for  
24 the selected bands for estimating  $GPP$  (i.e. 996 nm and 710 nm) are strongly correlated with  
25 canopy total chlorophyll content ( $R^2 > 0.80$ ).

### 26 **3.6 Band selection using GA-rF method**

27 Figure 10 shows the results of the band selection based on GA-rF method. In particular, each  
28 plot represents the frequency of the occurrence of each band in the genetic algorithm.

1 Overall, using the GA-rF method it was possible to identify portions of the spectrum that were of  
2 particular significance for estimating specific properties of the different ecosystems. For  
3 example, for predicting midday GPP (Fig. 10b) for all sites pooled together, the bands at 430 nm,  
4 630 nm, 660 nm and 710 nm showed the best results. The bands at 505 nm played an important  
5 role in predicting midday GPP for Amplero; bands at 660 nm for Neustift and bands 710 nm for  
6 Monte Bondone. Some differences were found for the different time resolutions (compare Figs.  
7 10b and 10c). For example, the bands at 580 nm and 800 nm showed the best results for  
8 Amplero and bands at 530 nm for Neustift.  
9 Figure 11 shows the results for the band selection by GA-rF methods for biophysical variables  
10 (i.e. dry phytomass, nitrogen and water content). For the variables related to slow processes the  
11 GA-rF method highlighted different bands for different sites; a much higher between site  
12 variability for the variables related to ecophysiological processes (e.g.  $\epsilon$ ,  $\alpha$  and  $GPP_{max}$ ) was  
13 detected and we weren't able to identify common "hot spots".

14

#### 15 **4 Discussion**

16 This study aimed at evaluating the potential of hyperspectral reflectance measurements to  
17 simulate CO<sub>2</sub> fluxes and ecophysiological variables of European mountain grasslands over a  
18 range of climatic conditions and management practices (grazing, harvest). To this end, we  
19 combined eddy covariance CO<sub>2</sub> flux measurements with ground-based hyperspectral  
20 measurements at six mountain grassland sites in Europe.

21

#### 22 *Up-scaling of in-situ relationships between VI indices and CO<sub>2</sub> fluxes and ecophysiological* 23 *parameters*

24 Despite the fact that we focused on a single type of ecosystem, our results showed that large  
25 differences existed among the investigated sites in the relationships between hyperspectral  
26 reflectance data and CO<sub>2</sub> fluxes and ecophysiological parameters. For all study sites pooled,  
27 hyperspectral reflectance data explained 40-68% of the variability in the dependent variables  
28 (Figs. 4-6). The conventional VIs yielded a maximum of 47% of explained variability in the data  
29 (Tables 3-4).

1 This is the first study comparing different grasslands characterized by different plant species and  
2 environmental conditions. The use of simple models based on a linear relationship between GPP  
3 and VIs, related to canopy greenness, has proven to be a good proxy for GPP of ecosystems with  
4 strong green-up and senescence (Peng et al., 2011; Rossini et al., 2012). The loss of this  
5 relationship may be related to low  $\epsilon$  variability due to abiotic and biotic stressors, the  
6 dependency of PRI on LAI, leaf and canopy biochemical structure (e.g. leaf orientation), and  
7 xanthophyll cycle inhibition or saturation and zeaxanthin-independent quenching (Gamon et al.,  
8 2001; Filella et al., 2004; Rahimzadeh-Bajgiran et al. 2012; Hmimina et al., 2014). For alpine  
9 grasslands, a key meteorological variable that played a relevant role in stimulating  $\epsilon$  was high  
10 soil water content associated with low temperatures (Polley et al. 2011). Low soil water contents  
11 triggered a decrease in leaf conductance as well as in  $\epsilon$  and in  $\alpha$  also for two oak and beech  
12 ecosystems (Hmimina et al., 2014). However, no significant differences in leaf biochemical and  
13 structural properties of the canopy at lowest and highest water content were found. In addition, in  
14 this special issue, Sakowska et al. (2014) showed that  $\epsilon$  is also strongly affected by the  
15 directional distribution of incident PAR, i.e. the ratio of direct to diffuse PAR.

16 Considering all sites pooled together (Figs. 4 and S1), NSD-type indices showed a very poor  
17 correlation in the VIS vs. NIR band combinations (i.e. traditional "greenness" indices, see Table  
18 2) with GPP. It is well-known in the literature (Rossini et al., 2010, 2012; Peng et al., 2010;  
19 Sakowska et al., 2014) that "greenness" indices, for grasslands and crops, are often good proxies  
20 of fAPARgreen (and thus carbon fluxes). Interestingly, in our study their performance was  
21 considerably poorer than expected. The NSD-type index showed a better performance in VIS vs.  
22 VIS band combinations than VIS vs. NIR ones. VIS vs. VIS band combination for NSD-type  
23 indices (e.g. green vs. blue or red, green vs. green wavelengths; see e.g. Inoue et al, 2008) are  
24 defined as "greenness" indices (Fig. 1), although their performance is generally much poorer  
25 than NSD VIS vs. NIR indices. These results are likely due to the confounding effects of the  
26 different canopy structures, and consequently of the different NIR response of the investigated  
27 grasslands (see Fig. 3). In fact, the different grassland structures (spatial distribution of  
28 photosynthetic, and also non photosynthetic material, leaf angles, etc.) is affecting our ability to  
29 use traditional indices to estimate fAPARgreen (and fluxes) when we consider different  
30 grasslands together because the structural effects on scattering are very complex in the NIR

1 (Jacquemoud et al., 2009; Knyazikhin et al., 2012). These results are of importance for the  
2 community, which still relies a lot on these relationships, also favoured by the availability of  
3 affordable narrow-band sensors that allow continuous monitoring of e.g. NDVI. These results  
4 suggest that waveband combinations not exploited by presently used (conventional) VIs may  
5 offer considerable potential for predicting grassland CO<sub>2</sub> fluxes, which has implications for the  
6 design and capabilities of future space/airborne or ground-based low cost sensors. In particular,  
7 these results also have a strong impact on our ability to up-scale grassland fAPAR<sub>green</sub> and  
8 carbon fluxes using upcoming sensors (e.g. Sentinel 2).

9 The evaluation of the models found for the main dataset against three new sites confirmed that  
10 these models can be transferred to predict carbon fluxes and ecophysiological parameters for  
11 similar grasslands (Fig. 8). However, these findings also challenge the current practice in up-  
12 scaling to larger regions by grouping all grasslands into a single plant functional type (PFT). We  
13 advocate more studies to be conducted merging CO<sub>2</sub> flux with hyperspectral data by means of  
14 models which use a more process-oriented and coupled approach to simulating canopy CO<sub>2</sub>  
15 exchange and reflectance in order to explore the causes underlying the observed differences  
16 between seemingly closely related study sites.

#### 17 *Grassland structural characteristic and their spectral response*

18 Although we considered similar ecosystems (belonging to the same vegetation type) the  
19 investigated canopies were very different and included Mediterranean, extensive alpine and  
20 intensive alpine grasslands with very different canopy structures in terms of leaf orientation,  
21 amount and spatial distribution of green and non-photosynthetic components, leaf nitrogen and  
22 water content as detailed in Vescovo et al. (2012).

23 For Amplero and Neustift NSD-type indices performed well for NIR vs. NIR band combinations  
24 for all investigated parameters, while Monte Bondone showed best performances in the VIS vs.  
25 NIR band combinations for GPP<sub>max</sub> and  $\epsilon$  (Fig. 7). The dry phytomass was the main driving factor  
26 of the spectral response in NIR vs. NIR band combinations for Amplero, while nitrogen content  
27 drove the spectral response in NIR vs. NIR band combinations of Neustift for all parameter  
28 except for  $\alpha$  (Tab. 5 and S3). Interestingly, for Monte Bondone both dry phytomass and nitrogen  
29 content explained the spectral response of the grassland in VIS vs. NIR band combinations for  
30

1 GPP<sub>max</sub> and  $\epsilon$  while no significant relationships with biophysical variables were found for  $\alpha$ ,  
2 GPP, NEE. These results partially confirm the findings of Vescovo et al. (2012), who  
3 highlighted a strong relationship, for several grassland types, between an NSD-type index and  
4 phytomass.

5 For Monte Bondone, NSD- and SR-type indices for the selected bands for estimating all  
6 variables except  $\alpha$  were strongly correlated with canopy total chlorophyll content ( $R^2 > 0.85$ ).

7 The chlorophyll indices (e.g. RedEdge NDVI and CI; see Tables 3 and 4) – which are considered  
8 the best indices for estimating carbon fluxes on grasslands and crops) – showed in our dataset a  
9 good performance for Amplero and Monte Bondone, but performed poorly for Neustift.

10 It was demonstrated by many authors that the red edge domain, where reflectance changes from  
11 very low in the absorption region to high in the NIR, is one of the best descriptors of chlorophyll  
12 concentration. On the other hand, it is well known that the canopy structure can be a very strong  
13 confounding factor. Our results confirm that this topic needs to be further investigated, as this  
14 finding has a relevant impact concerning the use of Sentinel 2 to upscale fAPAR and carbon flux  
15 observations.

16 It is interesting to see that the NSD-type indices in the NIR vs. NIR band combinations appeared  
17 to be the best proxy for GPP fluxes when all the grasslands were pooled together. These results  
18 can be linked to the controversial paper focused on the strong impact of structure on the ability to  
19 estimate canopy nitrogen content (Knyazikhin et al., 2012) and confirm the need for more  
20 studies in this direction. Good relationships were found between the NIR vs. NIR band  
21 combinations (>750nm wavelengths) and fluxes; the physical basis of these relationships need to  
22 be further investigated. In fact, it is important to highlight that the literature indicates that the  
23 wavelengths in the NIR (>750nm) are not sensitive to chlorophyll content, but they are related to  
24 leaf, canopy structure, and -around the 970nm area- to water.

25 As confirmed by comparing the correlation matrix approach with the GA-rF approach we  
26 couldn't find a universal relationship between reflectance in specific wavelengths of the light  
27 spectrum to biophysical properties of vegetation. We think that this is strongly linked to  
28 vegetation structure effects. For this reason we believe that further research for disentangling the

1 impact of factors like bidirectional reflectance distribution function and scaling effects is  
2 necessary.

3

## 4 **5 Conclusions**

5 The present study focused on understanding the potential of hyperspectral VIs in predicting  
6 grassland CO<sub>2</sub> exchange and ecophysiological parameters ( $\alpha$ ,  $\varepsilon$  and GPP<sub>max</sub>) for different  
7 European mountain grasslands.

8 The major finding of this study is that the relationship between ground-based hyperspectral  
9 reflectance and the ecosystem-scale CO<sub>2</sub> exchange of mountain grasslands is much more variable  
10 than what might be supposed given this closely related group of structurally and functionally  
11 similar ecosystems. As a consequence, the unique models of mountain grassland CO<sub>2</sub> exchange,  
12 i.e. the best fitting models for all sites pooled, explained 47% and 68% of the variability in the  
13 independent variables when established VIs and optimized hyperspectral VIs, respectively, were  
14 used. Interestingly, VIs based on reflectance either in the visible or NIR part of the  
15 electromagnetic spectrum were superior in predicting mountain grassland CO<sub>2</sub> exchange and  
16 ecophysiological parameters compared to commonly used VIs which are based on a combination  
17 of these two wavebands. **The band selection based on GA-rF algorithm confirmed that is difficult  
18 to define a universal band range able to describe ecophysiological parameters, carbon fluxes and  
19 biophysical variables even for a closely related group of ecosystems.**

20 The take-home message from this study thus is that continuing efforts are required to better  
21 understand differences in the relationship between ecosystem-scale reflectance and CO<sub>2</sub>  
22 exchange and to improve models of this relationship which can be employed to up-scale the land  
23 CO<sub>2</sub> exchange to larger spatial scales based on optical remote sensing data. Initiatives such as  
24 SpecNet (<http://specnet.info>; Gamon et al., 2006), the COST Action ES0903 (EUROSPEC;  
25 <http://cost-es0903.fem-environment.eu/>) and the COST Action ES1309 (OPTIMISE;  
26 [http://www.cost.eu/domains\\_actions/essem/Actions/ES1309](http://www.cost.eu/domains_actions/essem/Actions/ES1309)) are instrumental to this end as they  
27 provided the scale-consistent combination of hyperspectral reflectance and CO<sub>2</sub> exchange data.

28

## 29 **Acknowledgements**

1 MB acknowledges the support by the Methusalem program of the Flemish Government. LV and  
2 DG acknowledge the financial support obtained by the EU project CARBOEUROPE-IP (GOCE-  
3 CT-2003-505572) and the CARBOITALY project funded by the Italian Government. GW and AH  
4 acknowledge financial support by the Austrian National Science Fund (FWF) through grant  
5 agreements P17562 and P26425 and the Tyrolean Science Fund through grant agreement UNI-  
6 404/33. AH was financially supported through a DOC fellowship by the Austrian Academy of  
7 Sciences (ÖAW). ET acknowledges the support of the Province of Bolzano/Bozen through the  
8 project MONALISA.

9

## 10 **References**

11 Aubinet, M., Vesala, T., and Papale, D.: Eddy Covariance - A Practical Guide to Measurement  
12 and Data Analysis, Springer, ISBN: 978-94-007-2351-1, 2012.

13 Aubinet, M., Grelle, A., Ibrom, A., Rannik, U., Moncrieff, J., Foken, T., Kowalski, P., Martin,  
14 P., Berbigier, P., Bernhofer, C., Clement, R., Elbers, J., Granier, A., Grunwald, T., Morgenster,  
15 K., Pilegaard, K., Rebmann, C., Snijders, W., Valentini, R., and Vesala, T.: Estimates of the  
16 annual net carbon and water exchange of European forests: the EUROFLUX methodology,  
17 *Adv.Ecol.Res.*, 30, 113–75, 2000.

18 Bacour, C., Baret, F., and Jacquemoud, S.: Information content of HyMap hyperspectral  
19 imagery, *Proceedings of the 1st International Symposium on Recent Advances in Quantitative  
20 Remote Sensing, Valencia (Spain)*, 503–508, 2002.

21 Bacour, C., Jacquemoud, S., Leroy, M., Hautecoeur, O., Weiss, M., Prévot, L., Bruguier, L.,  
22 Chauki H.: Reliability of the estimation of vegetation characteristics by inversion of three  
23 canopy reflectance models on airborne POLDER data, *Agronomie*, 22, 555–565, 2002.

24 Baldocchi, D., Valentini, R., Running, S., Oechel, W., and Dahlman, R.: Strategies for  
25 measuring and modelling carbon dioxide and water vapour fluxes over terrestrial ecosystems,  
26 *Glob. Change Biol.*, 2, 159–168, 1996.

27 Balzarolo, M.: Biometric parameters and fluxes estimations in Mediterranean mountainous  
28 grassland with remote sensing techniques, PhD thesis, University of Tuscia, 2008.

29 Balzarolo, M., Anderson, K., Nichol, C., Rossini, M., Vescovo, L., Arriga, N., Wohlfahrt, G.,  
30 Calvet, J.-C., Carrara, A., Cerasoli, S., Cogliati, S., Daumard, F., Eklundh, L., Elbers, J. A.,  
31 Evrendilek, F., Handcock, R. N., Kaduk, J., Klumpp, K., Longdoz, B., Matteucci, G., Meroni,  
32 M., Montagnani, L., Ourcival, J.-M., Sanchez-Canete, E. P., Pontailier, J.-Y., Juszczak, R.,  
33 Scholes, B., and Pilar Martin, M.: Ground-based optical measurements at European flux sites: a  
34 review of methods, instruments and current controversies, *Sensors*, 11, 7954–7981, 2011.



- 1 Baret, F., Jacquemoud, S., Guyot, G., and Leprieur, C.: Modeled analysis of the biophysical  
2 nature of spectral shifts and comparison with information content of broad bands, *Remote Sens.*  
3 *Environ.*, 41, 133–142, 1992.
- 4 Barnes, J. D., Balaguer, L., Manrique, E., Elvira, S., and Davison, A. W.: A reappraisal of the  
5 use of DMSO for the extraction and determination of chlorophylls a and b in lichens and higher  
6 plants, *Environ. Exp. Bot.*, 32, 85–100, 1992.
- 7 Beer, C., Reichstein, M., Tomelleri, E., Ciais, P., Jung, M., Carvalhais, N., Rodenbeck, C.,  
8 Arain, M. A., Baldocchi, D., Bonan, G. B., Bondeau, A., Cescatti, A., Lasslop, G., Lindroth, A.,  
9 Lomas, M., Luysaert, S., Margolis, H., Oleson, K. W., Rouspard, O., Veenendaal, E., Viovy,  
10 N., Williams, C., Woodward, F. I., and Papale, D.: Terrestrial gross carbon dioxide uptake:  
11 global distribution and covariation with climate, *Science*, 329, 834–838,  
12 doi:10.1126/science.1184984, 2010.
- 13 Breiman, L., *Random Forests*, *Mach. Learn.*, 45, 5-32, 2001.
- 14 Cernusca, A., Bahn, M., Berninger, F., Tappeiner, U., Wohlfahrt, G.: Effects of land-use changes  
15 on sources, sinks and fluxes of carbon in European mountain grasslands, *Ecosystems*, 11:1335–  
16 1337, 2008.
- 17 Ciais, P., Wattenbach, M., Vuichard, N., Smith, P., Piao, S. L., Don, A., Luysaert, S., Janssens,  
18 I. A., Bondeau, A., Dechow, R., Leip, A., Smith, P. C., Beer, C., van der Werf, G. R., Gervois,  
19 S., Van Oost, K., Tomelleri, E., Freibauer, A., Schulze, E. D., and Team, C. S.: The european  
20 carbon balance. Part 2: Croplands, *Glob. Change Biol.*, 16, 1409–1428, 2010.
- 21 Clevers, J. G. P. W., Kooistra, L., and Schaepman, M.E.: Estimating canopy water content using  
22 hyperspectral remote sensing data, *Int. J. Appl. Earth Observ. Geoinform.*, 12, 119–125, 2010.
- 23 Clevers, J. G. P. W. and Gitelson, A. A.: Remote estimation of crop and grass chlorophyll and  
24 nitrogen content using red-edge bands on Sentinel-2 and -3, *Int. J. Appl. Earth Obs.*, 23, 10 344–  
25 351, doi:10.1016/j.jag.2012.10.008, 2013.
- 26 Colombo, R., Meroni, M., Marchesi, A., Busetto, L., Rossini, M., Giardino, C., and Panigada,  
27 C.: Estimation of leaf and canopy water content in poplar plantations by means of hyperspectral  
28 indices and inverse modeling, *Remote Sens. Environ.*, 112, 4, 1820-1834, 2008.
- 29 Coops, N. C., Hilker, T., Hall, F. G., Nichol, C. J., and Drolet, G. G.: Estimation of light-use  
30 efficiency of terrestrial ecosystem from space: a status report, *Bioscience*, 60, 788–797, 2010.
- 31 Drolet, G. G., Huemmrich, K. F., Hall, F. G., Middleton, E. M., Black, T. A., Black, T., Barr, A.,  
32 Barr, A. A., and Margolis, H.: A MODIS-derived photochemical reflectance index to detect  
33 interannual variations in the photosynthetic light-use efficiency of a boreal deciduous forest,  
34 *Remote Sens. Environ.*, 98, 212–224, doi:10.1016/j.rse.2005.07.006, 2005.
- 35 EEA, Agriculture and environment in EU-15. The IRENA Indicator Report, EEA, Copenhagen,  
36 ISBN 92-9167-779-5, 2005.
- 37 Fava, F., Colombo, R., Bocchi, S., Meroni, M., Sitzia, M., Fois, N., and Zucca, C.: Identification  
38 of hyperspectral vegetation indices for Mediterranean pasture characterization, *Int. J. Appl. Earth*  
39 *Obs. Geoinf.*, 11, 233–243, 2009.



- 1 Filella, I., Peñuelas, J., Llorens, L., and Estiarte, M.: Reflectance assessment of seasonal and  
2 annual changes in biomass and CO<sub>2</sub> uptake of a Mediterranean shrubland submitted to  
3 experimental warming and drought. *Remote Sens. Environ.*, 90, 308–318, 2004.
- 4 Frankenberg, C., Fisher, J. B., Worden, J., Badgley, G., Saatchi, S. S., Lee, J.-E., Toon, G. C.,  
5 Butz, A., Jung, M., Kuze, A., and Yokota, T.: New global observations of the terrestrial carbon  
6 cycle from GOSAT: patterns of plant fluorescence with gross primary productivity, *Geophys.*  
7 *Res. Lett.*, 38, L17706, doi:10.1029/2011gl048738, 2011.
- 8 Gamon, J. A., Peñuelas, J., and Field, C. B.: A narrow-waveband spectral index that tracks  
9 diurnal changes in photosynthetic efficiency, *Remote Sens. Environ.*, 41, 35–44, 1992.
- 10 Gamon, J. A., Field, C. B., Fredeen, A. L., and Thayer, S.: Assessing photosynthetic  
11 downregulation in sunflower stands with an optically-based model. *Plant Biology* 67, 113–125,  
12 2001.
- 13 Gamon, J. A., Rahman, A. F., Dungan, J. L., Schildhauer, M., Huemmrich, K. F.: Spectral  
14 Network (SpecNet): What Is It and Why Do We Need It?, *Remote Sens. Environ.* 103, 227-235,  
15 2006.
- 16 Gamon, J. A., Coburn, C., Flanagan, L. B., Huemmrich, K. F., Kiddle, C., Sanchez-Azofeifa, G.  
17 A., Thayer, D. R., Vescovo, L., Gianelle, D., Sims, D. A., Rahman, A. F., and Pastorello, G. Z.:  
18 SpecNet revisited: bridging flux and remote sensing communities, *Can. J. Remote Sens.*, 36,  
19 S376–S390, 2010.
- 20 Garbulsky, M. F., Peñuelas, J., Gamon, J., Inoue, Y., and Filella, I.: The photochemical  
21 reflectance index (PRI) and the remote sensing of leaf, canopy and ecosystem radiation use  
22 efficiencies –a review and meta-analysis, *Remote Sens. Environ.*, 115, 281–297, 2011.
- 23 Gianelle, D., Vescovo, L., Marcolla, B., Manca, G., and Cescatti, A.: Ecosystem carbon fluxes  
24 and canopy spectral reflectance of a mountain meadow, *Int. J. Remote Sens.*, 30, 435–449, 2009.
- 25 Gilmanov, T. G., Soussana, J. F., Aires, L., Allard, V., Ammann, C., Balzarolo, M., Barcza, Z.,  
26 Bernhofer, C., Campbell, C. L., Cernusca, A., Cescatti, A., Clifton-Brown, J., Dirks, B. O. M.,  
27 Dore, S., Eugster, W., Fuhrer, J., Gimeno, C., Gruenwald, T., Haszpra, L., Hensen, A., Ibrom,  
28 A., Jacobs, A. F. G., Jones, M. B., Lanigan, G., Laurila, T., Lohila, A., Manca, G., Marcolla, B.,  
29 Nagy, Z., Pilegaard, K., Pinter, K., Pio, C., Raschi, A., Rogiers, N., Sanz, M. J., Stefani, P.,  
30 Sutton, M., Tuba, Z., Valentini, R., Williams, M. L., and Wohlfahrt, G.: Partitioning European  
31 grassland net ecosystem CO<sub>2</sub> exchange into gross primary productivity and ecosystem  
32 respiration using light response function analysis, *Agr. Ecosyst. Environ.*, 121, 93–120, 2007.
- 33 Gitelson, A. A., and Merzlyak, M. N.: Remote estimation of chlorophyll content in higher plant  
34 leaves. *Int. J. Remote Sens.*, 18, 2691–2697, 1997.
- 35 Gitelson, A. A., Viña, A., Ciganda, V., Rundquist, D. C., and Arkebauer, T. J.: Remote  
36 estimation of canopy chlorophyll content in crops, *Geophys. Res. Lett.*, 32, L08403,  
37 doi:10.1029/2005GL022688, 2005.
- 38 Gitelson, A. A., Viña, A., Rundquist, D. C., Arkebauer, T. J., Keydan, G., Leavitt, B., Ciganda,  
39 V., Burba, G. G., and Suyker, A. E.: Relationship between gross primary production and  
40 chlorophyll content in crops: Implications for the synoptic monitoring of vegetation productivity,  
41 *Geophys. Res. Lett.*, 111, D08S11. <http://dx.doi.org/10.1029/2005JD006017>, 2006.

- 1 Gitelson, A.A., Vina, A., Masek, J.G., Verma, S. B., and Suyker, A.E.: Synoptic monitoring of  
2 gross primary productivity of maize using Landsat data, *IEEE Geosci. Remote S.*, 5, 133–137,  
3 2008.
- 4 Gitelson, A. A., Peng, Y., Masek, J. G., Rundquist, D. C., Verma, S., Suyker, A., Baker, J. M.,  
5 Hatfield, J. L., and Meyers, T.: Remote estimation of crop gross primary production with  
6 Landsat data, *Remote Sens. Environ.*, 121, 404–414, doi:10.1016/j.rse.2012.02.017, 2012.
- 7 Goerner, A., Reichstein, M., Tomelleri, E., Hanan, N., Rambal, S., Papale, D., Dragoni, D., and  
8 Schmullius, C.: Remote sensing of ecosystem light use efficiency with MODIS-based PRI,  
9 *Biogeosciences*, 8, 189–202, 2011.
- 10 [Grossman, Y. L., Ustin, S. L., Sanderson, E., Jacquemoud, J., Schmuck, G., and Verdebout J.:](#)  
11 [Critique of stepwise multiple linear regression for the extraction of leaf biochemistry information](#)  
12 [from leaf reflectance data, \*Remote Sens. Environ.\*, 56, 182–193, 1996.](#)
- 13 Hatfield, J. L. Gitelson, A. A., Schepers, J. S., and Walthall, C. L.: Application of spectral  
14 remote sensing for agronomic decisions, *Agron. J.*, 100,117–131, doi:10.2134/agronj2006.0370c,  
15 2008.
- 16 Heinsch, F. A., Zhao, M. S., Running, S. W., Kimball, J. S., Nemani, R. R., Davis, K. J., Bolstad,  
17 P. V., Cook, B. D., Desai, A. R., Ricciuto, D. M., Law, B. E., Oechel, W. C., Kwon, H., Luo, H.  
18 Y., Wofsy, S. C., Dunn, A. L., Munger, J. W., Baldocchi, D. D., Xu, L. K., Hollinger, D. Y.,  
19 Richardson, A. D., Stoy, P. C., Siqueira, M. B. S., Monson, R. K., Burns, S. P., and Flanagan, L.  
20 B.: Evaluation of remote sensing based terrestrial productivity from MODIS using regional  
21 tower eddy flux network observations, *IEEE T. Geosci. Remote*, 44, 1908–1925, 2006.
- 22 Hmimina, G., Dufrêne, E., and Soudani, K.: Relationship between photochemical reflectance  
23 index and leaf ecophysiological and biochemical parameters under two different water statuses:  
24 towards a rapid and efficient correction method using real-time measurements, *Plant Cell*  
25 *Environ.*, 37, 473–487, 2014.
- 26 Inoue, Y., Peñuelas, J., Miyata, A., and Mano, M.: Normalized difference spectral indices for  
27 estimating photosynthetic efficiency and capacity at a canopy scale derived from hyperspectral  
28 and CO<sub>2</sub> flux measurements in rice, *Remote Sens. Env.*, 112, 156–172, 2008.
- 29 [Jacquemoud, S., and Baret, F.: PROSPECT: a model of leaf optical properties spectra, \*Remote\*](#)  
30 [Sens. Environ., 34, 75–91, 1990.](#)
- 31 [Jacquemoud, S.: Inversion of the PROSPECT+SAIL canopy reflectance model from AVIRIS](#)  
32 [equivalent spectra: Theoretical study, \*Remote Sens. Environ.\*, 44, 281–292, 1993.](#)
- 33 [Jacquemoud, S., Bacour, C., Poilvé, H., and Frangi, I.-P.: Comparison of four radiative transfer](#)  
34 [models to simulate plant canopies reflectance: direct and inverse mode, \*Remote Sens. Env.\*, 74,](#)  
35 [471–481, 2000.](#)
- 36 Jordan, C. F.: Derivation of leaf area index from quality of light on the forest floor, *Ecology*, 50,  
37 663–666, 1969.

- 1 Kiniry, J. R., Burson, B. L., Evers, G. W., Williams, J. R., Sanchez, H., Wade, C., Featherston, J.  
2 W., and Greenwade J.: Coastal bermudagrass, bahiagrass, and native range simulation for  
3 diverse sites in Texas, *Agron. J.*, 99, 450–61, 2007.
- 4 Knyazikhin, Y., Schull, M. A., Stenberg, P., Mörtus, M., Rautiainen, M., Yang, Y., Marshak, A.,  
5 Latorre Carmona, P., Kaufmann, R. K., Lewis, P., Disney, M. I., Vanderbilt, V., Davis, A. B.,  
6 Baret, F., Jacquemoud, S., Lyapustin, A., and Myneni, R. B. : Hyperspectral remote sensing of  
7 foliar nitrogen content, *Proc. Natl. Acad. Sci. USA*, 110, 185–192, 2012.
- 8 Lambers, H., Chapin III, F. S., and Pons, T.L.: *Plant physiological ecology*, Springer-Verlag,  
9 Berlin, 540, 1998.
- 10 Li, L., Ustin, S. L., Riano, D.: Retrieval of fresh leaf fuel moisture content using genetic  
11 algorithm – partial least squares modeling (GA-PLS). *EEE T. Geosci. Remote Letters*, 4, 216–  
12 220, 2007.
- 13 Lichtenthaler, H. K: *Chlorophylls and carotenoids: Pigments of photosynthetic biomembranes*,  
14 *Methods in Enzymology*, 148, 349–382, 1987.
- 15 Marquardt, D. W.: An Algorithm for Least-Squares Estimation of Nonlinear Parameters, *SIAM*  
16 *J. Appl. Math.*, 11, 431–441, doi:10.1137/0111030, 1963.
- 17 Mauder, M., Foken, T., Bernhofer, C., Clement, R., Elbers, J., Eugster, W., Grünwald, T.,  
18 Heusinkveld, B., and Kolle, O.: Quality control of CarboEurope flux data – Part 2: Inter-  
19 comparison of eddy-covariance software, *Biogeosciences*, 5, 451–462, 2008,  
20 <http://www.biogeosciences.net/5/451/2008/>.
- 21 Meroni, M., Rossini, M., Guanter, L., Alonso, L., Rascher, U., Colombo, R., and Moreno, J.:  
22 Remote sensing of solar induced chlorophyll fluorescence: review of methods and applications,  
23 *Remote Sens. Environ.*, 113, 2037–2051, 2009.
- 24 Meroni, M., Barducci, A., Cogliati, S., Castagnoli, F., Rossini, M., Busetto, L., Migliavacca, M.,  
25 Cremonese, E., Galvagno, M., Colombo, R., and Morra di Cella, U.: The hyperspectral  
26 irradiometer, a new instrument for long-term and unattended field spectroscopy measurements,  
27 *Rev. Sci. Instrum.* 82, 043106; 2011; <http://dx.doi.org/10.1063/1.3574360>.
- 28 Monteith, J. L.: Solar radiation and productivity in tropical ecosystems, *J. Appl. Ecol.*, 9(3), 747–  
29 766, 1972.
- 30 Monteith, J. L. and Moss, C. J.: Climate and the Efficiency of Crop Production in Britain, *Philos.*  
31 *Trans. R. Soc. London B Biol. Sci.*, 281, 277–294, doi:10.1098/rstb.1977.0140, 1977.
- 32 Moore, C.J.: Frequency response corrections for eddy correlation systems, *Bound.-Lay.*  
33 *Meteorol.*, 37, 17–35, 1986.
- 34 Nichol, C. J., Lloyd, J., Shibistova, O., Arneth, A., Roser, C., Knohl, A., Matsubara, S., and  
35 Grace, J.: Remote sensing of photosynthetic-light-use efficiency of a Siberian boreal forest,  
36 *Tellus B*, 54, 677–687, 2002.
- 37 Ollinger, S. V., Richardson, A. D., Martin, M. E., Hollinger, D. Y., Frohking, S., Reich, P. B.,  
38 Plourde, L. C., Katul, G. G., Munger, J.W., Oren, R., Smith, M.-L., Paw U, K. T., Bolstad, P. V.,  
39 Cook, B. D., Day, M. C., Martin, T. A., Monson, R. K., and Schmid, H. P.: Canopy nitrogen,  
40 carbon assimilation, and albedo in temperate and boreal forests: functional relations and potential

- 1 [climate feedbacks](#), *P. Natl. Acad. Sci. USA*, 105, 19336–19341, doi:10.1073/pnas.0810021105,  
2 2008.
- 3 Peng, Y., Gitelson, A. A., Keydan, G., Rundquist, D. C., and Moses, W.: Remote estimation of  
4 gross primary production in maize and support for a new paradigm based on total crop  
5 chlorophyll content, *Remote Sens. Environ.*, 115, 978–989, 2011.
- 6 Peñuelas, J., Filella, I., Biel, C., Serrano, L., and Save, R.: The reflectance at the 950-970 nm  
7 region as an indicator of plant water status, *Int. J. Remote Sens.*, 14, 1887–1905, 1993.
- 8 Peñuelas, J., Gamon, J. A., Fredeen, A., Merino, J., and Field, C. B.: Reflectance indices  
9 associated with physiological changes in nitrogen- and water-limited sunflower leaves. *Remote  
10 Sens. Environ.*, 48, 135–146, 1994.
- 11 Peñuelas, J., Filella, I., and Gamon, J. A.: Assessment of photosynthetic radiation-use efficiency  
12 with spectral reflectance, *New Phytol.*, 131, 291–296, 1995.
- 13 Peñuelas, J., and Filella, I.: Visible and near-infrared reflectance techniques for diagnosing plant  
14 physiological status, *Trends Plant Sci.*, 3, 151–156, 1998.
- 15 [Peñuelas, J., Garbulsky, M. F., and Filella, I.: Photochemical reflectance index \(PRI\) and remote  
16 sensing of plant CO<sub>2</sub> uptake](#), *New Phytol.*, 191, 596–599, 2011.
- 17 Polley, H. W., Phillips, B. L., Frank, A. B., Bradford, J. A., Sims, P. L., Morgan, J. A., and  
18 Kiniry, J. R.: Variability in light-use efficiency for gross primary productivity on Great Plains  
19 grasslands, *Ecosystems*, 14, 15–27, 2011.
- 20 Rahimzadeh-Bajgiran, P., Munehiro, M., and Omasa, K.: Relationships between the  
21 photochemical reflectance index (PRI) and chlorophyll fluorescence parameters and plant  
22 pigment indices at different leaf growth stages. *Photosynt. Res.*, 113, 261–271, 2012.
- 23 Reichstein, M., Falge, E., Baldocchi, D., Papale, D., Valentini, R., Aubinet, M., Berbigier, P.,  
24 Bernhofer, C., Buchmann, N., Gilmanov, T., Granier, A., Grünwald, T., Havrankova, K., Janous,  
25 D., Knohl, A., Laurela, T., Lohila, A., Loustau, D., Matteucci, G., Meyers, T., Miglietta, F.,  
26 Ourcival, J.-M., Rambal, S., Rotenberg, E., Sanz, M., Seufert, G., Vaccari, F., Vesala, T., and  
27 Yakir, D.: On the separation of net ecosystem exchange into assimilation and ecosystem  
28 respiration: review and improved algorithm, *Glob. Change Biol.*, 11, 1424–1439, 2005.
- 29 [Riaño, D., Ustin, S. L., Usero, L., Patricio, M. A.: Estimation of fuel moisture content using  
30 neural networks](#). *Lect. Notes in Comput. Sc.*, 3562: 489–498, 2005a.
- 31 Rossini, M., Meroni, M., Migliavacca, M., Manca, G., Cogliati, S., Busetto, L., Picchi, V.,  
32 Cescatti, A., Seufert, G., and Colombo, R.: High resolution field spectroscopy measurements for  
33 estimating gross ecosystem production in a rice field, *Agr. Forest Meteorol.*, 150, 1283–1296,  
34 2010.
- 35 Rossini, M., Cogliati, S., Meroni, M., Migliavacca, M., Galvagno, M., Busetto, L., Cremonese,  
36 E., Julitta, T., C. Siniscalco, C., Morra di Cella, U., and Colombo, R.: Remote sensing-based  
37 estimation of gross primary production in a subalpine grassland, *Biogeosciences*, 9, 2565–2584,  
38 2012.
- 39 Rouse, J. W., Haas, R. H., Schell, J. A., and Deering, D. W.: Monitoring vegetation systems in  
40 the Great Plains with ERTS. 3rd ERTS Symposium, NASA SP-351 I, 1973.

- 1 Sakowska, K., Vescovo, L., Marcolla, B., Juszczak, R., Olejnik, J., and Gianelle, D.: Monitoring  
2 of carbon dioxide fluxes in a subalpine grassland ecosystem of the Italian Alps using a  
3 multispectral sensor, *Biogeosciences*, 11, 4695–4712, doi:10.5194/bg-11-4695-2014, 2014.
- 4 Schotanus, P., Nieuwstadt, F. T. M., and De Bruin H. A. R.: Temperature measurement with a  
5 sonic anemometer and its application to heat and moisture fluxes, *Bound. Lay. Meteorol.*, 26 81–  
6 93, 1983.
- 7 Schwalm, C. R., Black, T. A., Arniro, B. D., Arain, M. A., Barr, A. G., Bourque, C. P. A., et al.:  
8 Photosynthetic light use efficiency of three biomes across an East–west continental-scale transect  
9 in Canada, *Agric. For. Meteorol.*, 140, 269–286, 2006.
- 10 Sims, D. A., and Gamon, J. A.: Relationships between leaf pigment content and spectral  
11 reflectance across a wide range of species, leaf structures, and developmental stages, *Remote  
12 Sens. Env.*, 81, 337–354, 2002.
- 13 Soudani, K., Hmimina, G., Dufrêne, E., Berveiller, D., Delpierre, N., Ourcival, J.-M., Rambal,  
14 S., and Joffre, R.: Relationships between photochemical reflectance index and light-use  
15 efficiency in deciduous and evergreen broadleaf forests, *Remote Sens. Env.*, 144, 73–84, 2014.
- 16 Soussana, J. F., Allard, V., Pilegaard, K., Ambus, C., Campbell, C., Ceschia, E., Clifton-Brown,  
17 J., Czobel, S., Domingues, R., Flechard, C., Fuhrer, J., Hensen, A., Horvath, L., Jones, M.,  
18 Kasper, G., Martin, C., Nagy, Z., Neftel, A., Raschi, A., Baronti, S., Rees, R. M., Skiba, U.,  
19 Stefani, P., Manca, G., Sutton, M., Tuba, Z., and Valentini, R.: Full accounting of the greenhouse  
20 gas (CO<sub>2</sub>, N<sub>2</sub>O, CH<sub>4</sub>) budget of nine European grassland sites, *Agri. Eco. Enviro.*, 121, 121–134,  
21 2007.
- 22 Verhoef, W.: Light scattering by leaves with application to canopy reflectance modelling: the  
23 SAIL model, *Remote Sens. Environ.*, 16, 125–178, 1984.
- 24 Vescovo L., Wohlfahrt, G., Balzarolo, M., Pilloni, S., Sottocornola, M., Rodeghiero, M., and  
25 Gianelle, D.: New spectral vegetation indices based on the near-infrared shoulder wavelengths  
26 for remote sensing detection of grassland phytomass, *Int. J. Remote Sens.*, 33, 7, 2012.
- 27 Waring, R., and Running, S. W.: *Forest Ecosystems: Analysis at Multiple Scales*, Elsevier, New  
28 York, 1998.
- 29 Webb, E. K., Pearman, G. I., and Leuning, R.: Correction of flux measurements for density  
30 effects due to heat and water vapour transfer, *Q. J. Roy. Meteorol. Soc.*, 106, 85–100, 1980.
- 31 Vickers, D. and Mahrt, L.: Quality control and flux sampling problems for tower and aircraft  
32 data, *J. Atmos. Oceanic. Tech.*, 14, 512–526, 1997.
- 33
- 34 Wilczak, J. M., Oncley, S. P., and Stage, S. A.: Sonic anemometer tilt correction algorithms,  
35 *Bound.-Lay. Meteorol.*, 99, 127–150, 2001.
- 36 Wohlfahrt, G., Sapinsky, S., Tappeiner, U., and Cernusca, A.: Estimation of plant area index of  
37 grasslands from measurements of canopy radiation profiles, *Agr. Forest Meteorol.*, 109, 1–12,  
38 2001.

- 1 Wohlfahrt, G., Anderson-Dunn, M., Bahn, M., Balzarolo, M., Berninger, F., Campbell, C.,  
2 Carrara, A., Cescatti, A., Christensen, T., Dore, S., Eugster, W., Friborg, T., Furger, M.,  
3 Gianelle, D., Gimeno, C., Hargreaves, K., Hari, P., Haslwanter, A., Johansson, T., Marcolla, B.,  
4 Milford, C., Nagy, Z., Nemitz, E., Rogiers, N., Sanz, M.J., Siegwolf, R. T. W., Susiluoto, S.,  
5 Sutton, M., Tuba, Z., Ugolini, F., Valentini, R., Zorer, R., and Cernusca, A.: Biotic, abiotic and  
6 management controls on the net ecosystem CO<sub>2</sub> exchange of European mountain grasslands,  
7 *Ecosystems*, 11, 1338–1351, 2008.
- 8 Wohlfahrt, G., Pilloni, S., Hörtnagl, L., and Hammerle, A.: Estimating carbon dioxide fluxes  
9 from temperate mountain grasslands using broad-band vegetation indices, *Biogeosciences*, 7,  
10 683–694, doi:10.5194/bg-7-683-2010, 2010.
- 11 [Zarco-Tejada, P. J., Rueda, C. A., and Ustin, S. L.: Water content estimation in vegetation with](#)  
12 [MODIS reflectance data and model inversion method, \*Remote Sens. Env.\*, 85, 109–124, 2003.](#)
- 13

1 Table 1. Description of the study sites and period.

<i>Site characteristics</i>	Amplero (IT-Amp)	Neustift (AT-Neu)	Monte Bondone (IT-MBo)
Latitude	41.9041	47.1162	46.0296
Longitude	13.6052	11.3204	11.0829
Elevation (m)	884	970	1550
Mean annual temperature (°C)	10.0	6.5	5.5
Mean annual precipitation (mm)	1365	852	1189
Vegetation type	Seslerietum apenninae	Pastinaco– Arrhenatheretum	Nardetum Alpigenum
Study period <sup>1</sup>	111-170, 2006 (9)	122-303, 2006 (16)	129-201, 2005 (13) 124-192, 2006 (12)
Sonic anemometer model	R3, Gill, Gill Instruments Ltd., Lymington, UK	R3, Gill, Instruments Ltd., Lymington, UK	R3, Gill Instruments Ltd., Lymington, UK
Infrared gas analyser model	Li-7500, Li-Cor Inc., Lincoln, Nebraska, USA	Li-7500, Li-Cor Inc., Lincoln, Nebraska, USA	Li-7500, Li-Cor Inc., Lincoln, Nebraska, USA
Data acquisition frequency (Hz)	20	20	20
Post-processing software	Developped by University of Viterbo (IT)	EdiRE (Version 1.4.3.1021, R. Clement, University of Edinburgh)	EdiRE (Version 1.4.3.1021, R. Clement, University of Edinburgh)
Outlier removal (method)	Wickers and Mahrt (1997)	-	-

	Covariance maximization	Covariance maximization	Covariance maximization
CO <sub>2</sub> /H <sub>2</sub> O signal lag removal			
Coordinate rotation (method) <sup>2</sup>	3D	3D	3D
Detrending of time series (method)	Linear detrending	-	-
Density corrections applied <sup>3</sup>	x	x	x
Sonic buoyancy to sensible heat flux conversion and cross-wind correction <sup>4</sup>	x	x	x
Low- and high-pass filtering corrected for (method)	Aubinet et al. (2000)	Moore (1986)	Aubinet et al. (2000)
Iterative calculation of fluxes <sup>5</sup>	-	x	-

1 <sup>1</sup> from-to DOY, year (number of hyperspectral measurement dates); <sup>2</sup> according to Wilczak et al. (2001); <sup>3</sup> according to Webb et al. (1980); <sup>4</sup> according to  
2 Schotanus et al. (1983); <sup>5</sup> according to Mauder et al. (2008)

3

4

5



Table 2. Summary of the vegetation indices characteristics used in this study.

Index name and acronym	Formula	Use	Reference
<b><i>Simple Spectral Ratio Indices</i></b>			
Simple Ratio (SR or RVI)	$SR = R_{830}/R_{660}$	Greenness	Jordan (1969)
Green Ratio Index (GRI)	$GRI = R_{830}/R_{550}$	Greenness	Peñuelas and Filella (1998)
Water Index (WI)	$WI = R_{900}/R_{970}$	Water content, leaf water potential, canopy water content	Peñuelas et al. (1993)
Simple Ratio Pigment Index (SRPI)	$SRPI = (R_{430})/(R_{680})$		Peñuelas et al. (1995)
Chlorophyll Index (CI)	$CI = (R_{750}/R_{720}) - 1$	Chlorophyll content	Gitelson et al. (2005)
<b><i>Normalized Spectral Difference Vegetation Indices</i></b>			
Normalized Difference Vegetation Index (NDVI)	$NDVI = (R_{830} - R_{660}) / (R_{830} + R_{660})$	Greenness	Rouse et al. (1973)
Normalized Phaeophytinization Index (NPQI)	$NPQI = (R_{415} - R_{435}) / (R_{415} + R_{435})$	Carotenoid /Chlorophyll ratio	Barnes et al. (1992)
Normalized Pigment Chlorophyll Index (NPCI)	$NPCI = (R_{680} - R_{430}) / (R_{680} + R_{430})$	Chlorophyll ratio	Peñuelas et al. (1994)
Red-edge NDVI (Red-edge NDVI)	$Red-edge\ NDVI = (R_{750} - R_{720}) / (R_{750} + R_{720})$	Chlorophyll content	Gitelson and Merzlyak (1994)
Structural Independent Pigment Index (SIPI)	$SIPI = (R_{800} - R_{445}) / (R_{800} + R_{445})$	Chlorophyll content	Peñuelas et al. (1995)

Table 3. Results of statistic of linear regression models between VIs and ecophysiological parameters:  $\alpha$ ,  $\varepsilon$  (midday average) and  $GPP_{max}$ .  $R^2$ —Coefficient of determination; and RMSE—Root Mean Square Error. Bold letters indicate the best fitting model.

VI	$\alpha$								$\varepsilon$								$GPP_{max}$							
	Amplero		Neustift		Monte Bondone		All		Amplero		Neustift		Monte Bondone		All		Amplero		Neustift		Monte Bondone		All	
	$R^2$	RMSE	$R^2$	RMSE	$R^2$	RMSE	$R^2$	RMSE	$R^2$	RMSE	$R^2$	RMSE	$R^2$	RMSE	$R^2$	RMSE	$R^2$	RMSE	$R^2$	RMSE	$R^2$	RMSE	$R^2$	RMSE
	-	$\frac{\mu mol_{CO_2}}{\mu mol_{phot}}$	-	$\frac{\mu mol_{CO_2}}{\mu mol_{phot}}$	-	$\frac{\mu mol_{CO_2}}{\mu mol_{phot}}$	-	$\frac{\mu mol_{CO_2}}{\mu mol_{phot}}$	-	$\frac{\mu mol_{CO_2}}{\mu mol_{phot}}$	-	$\frac{\mu mol_{CO_2}}{\mu mol_{phot}}$	-	$\frac{\mu mol_{CO_2}}{\mu mol_{phot}}$	-	$\frac{\mu mol_{CO_2}}{\mu mol_{phot}}$	-	$\frac{\mu mol_{CO_2}}{\mu mol_{phot}}$	-	$\frac{\mu mol_{CO_2}}{\mu mol_{phot}}$	-	$\frac{\mu mol_{CO_2}}{\mu mol_{phot}}$	-	$\frac{\mu mol_{CO_2}}{\mu mol_{phot}}$
SR	0.57	0.01	0.04	0.07	<b>0.13</b>	0.01	0.06	0.04	0.50	0.01	0.33	0.03	0.35	0.04	0.18	0.04	<b>0.89</b>	1.58	0.01	4.31	0.78	2.76	0.28	6.71
GRI	0.29	0.01	0.00	0.07	0.13	0.01	0.00	0.05	0.26	0.01	<b>0.67</b>	0.02	0.44	0.04	<b>0.47</b>	0.03	0.69	2.66	0.00	4.35	0.81	2.53	0.09	7.51
WI	0.50	0.01	0.01	0.07	0.08	0.01	0.03	0.04	0.41	0.01	0.22	0.03	0.36	0.04	0.25	0.04	0.86	1.82	0.16	3.99	0.54	3.95	0.24	6.87
NDVI	0.44	0.01	0.04	0.07	0.06	0.01	0.06	0.04	0.40	0.01	0.30	0.03	0.53	0.04	0.43	0.03	0.79	2.21	0.03	4.28	<b>0.82</b>	2.50	0.37	6.27
SIPI	0.37	0.01	<b>0.07</b>	0.07	0.02	0.01	0.18	0.04	0.35	0.01	0.29	0.03	<b>0.64</b>	0.03	0.44	0.03	0.66	2.80	0.06	4.21	0.74	2.96	<b>0.47</b>	5.74
CI	0.49	0.01	0.00	0.07	0.09	0.01	0.01	0.05	0.41	0.01	0.65	0.02	0.43	0.04	0.34	0.04	0.81	2.08	0.01	4.34	0.80	2.62	0.16	7.24
PRI	<b>0.71</b>	0.01	0.02	0.07	0.02	0.01	0.14	0.04	0.50	0.01	0.19	0.03	0.28	0.05	0.40	0.04	0.41	3.68	<b>0.26</b>	3.75	0.11	5.50	0.14	7.33
EVI	0.47	0.01	0.03	0.07	0.03	0.01	0.14	0.04	0.46	0.01	0.43	0.03	0.53	0.04	0.38	0.04	0.78	2.25	0.01	4.33	0.70	3.21	0.32	6.50
NPQI	0.06	0.01	0.06	0.07	0.05	0.01	0.31	0.04	0.04	0.01	0.30	0.03	0.17	0.05	0.11	0.04	0.00	4.78	0.07	4.20	0.21	5.17	0.14	7.31
NPCI	0.50	0.01	0.07	0.07	0.03	0.01	<b>0.37</b>	0.04	0.51	0.01	0.17	0.03	0.00	0.05	0.00	0.05	0.53	3.28	0.17	3.97	0.17	5.33	0.32	6.52
SRPI	0.51	0.01	0.06	0.07	0.03	0.01	0.36	0.04	<b>0.56</b>	0.01	0.15	0.04	0.00	0.05	0.00	0.05	0.50	3.38	0.17	3.97	0.17	5.31	0.28	6.69
RedEdgeNDVI	0.48	0.01	0.00	0.07	0.07	0.01	0.01	0.05	0.40	0.01	0.65	0.02	0.47	0.04	0.40	0.04	0.79	2.16	0.00	4.34	0.80	2.58	0.19	7.09

Table 4. Results of statistic of linear regression models between VIs and midday average CO<sub>2</sub> fluxes: NEE and GPP. R<sup>2</sup>—Coefficient of determination; and RMSE—Root Mean Square Error. Bold letters indicate the best fitting model.

	GPP								NEE							
	Amplero		Neustift		Monte Bondone		All		Amplero		Neustift		Monte Bondone		All	
	R <sup>2</sup>	RMSE	R <sup>2</sup>	RMSE	R <sup>2</sup>	RMSE	R <sup>2</sup>	RMSE	R <sup>2</sup>	RMSE	R <sup>2</sup>	RMSE	R <sup>2</sup>	RMSE	R <sup>2</sup>	RMSE
	-	$\frac{\mu\text{mol}_{\text{CO}_2}}{\text{m}^2\text{s}}$	-	$\frac{\mu\text{mol}_{\text{CO}_2}}{\text{m}^2\text{s}}$	-	$\frac{\mu\text{mol}_{\text{CO}_2}}{\text{m}^2\text{s}}$	-	$\frac{\mu\text{mol}_{\text{CO}_2}}{\text{m}^2\text{s}}$	-	$\frac{\mu\text{mol}_{\text{CO}_2}}{\text{m}^2\text{s}}$	-	$\frac{\mu\text{mol}_{\text{CO}_2}}{\text{m}^2\text{s}}$	-	$\frac{\mu\text{mol}_{\text{CO}_2}}{\text{m}^2\text{s}}$	-	$\frac{\mu\text{mol}_{\text{CO}_2}}{\text{m}^2\text{s}}$
SR	0.86	1.59	0.08	4.56	0.75	3.12	0.27	7.09	0.36	2.76	0.08	4.77	0.68	3.19	0.18	6.35
GRI	0.85	1.67	0.01	4.44	0.80	2.78	0.10	7.85	<b>0.54</b>	2.32	0.01	4.96	0.68	3.21	0.08	6.73
WI	<b>0.92</b>	1.23	0.05	3.25	0.50	4.41	0.24	7.20	0.44	2.57	0.05	4.87	0.43	4.28	0.17	6.42
NDVI	0.82	1.79	<b>0.14</b>	4.58	0.80	2.82	0.36	6.60	0.42	2.63	<b>0.14</b>	4.63	0.72	3.01	0.29	5.94
SIPI	0.65	2.50	0.08	4.57	0.72	3.32	<b>0.46</b>	6.08	0.33	2.82	0.08	4.79	0.65	3.34	<b>0.39</b>	5.51
CI	0.88	1.44	0.00	4.31	0.81	2.69	0.17	7.56	0.43	2.59	0.00	4.98	<b>0.75</b>	2.82	0.12	6.59
PRI	0.25	3.69	0.05	4.34	0.14	5.79	0.10	7.84	0.00	3.44	0.05	4.87	0.15	5.20	0.05	6.84
EVI	0.75	2.11	0.01	4.31	0.68	3.51	0.33	6.79	0.36	2.74	0.01	4.97	0.71	3.03	0.26	6.05
NPQI	0.04	4.17	0.08	4.27	0.14	5.78	0.16	7.57	0.24	2.99	0.08	4.78	0.19	5.08	0.12	6.60
NPCI	0.40	3.29	0.01	4.45	0.14	5.76	0.30	6.92	0.11	3.25	0.01	4.95	0.21	5.03	0.25	6.09
SRPI	0.35	3.42	0.01	4.44	0.15	5.74	0.27	7.08	0.08	3.30	0.01	4.95	0.22	5.01	0.22	6.19
RedEdgeNDVI	0.87	1.51	0.00	4.35	<b>0.81</b>	2.68	0.20	7.40	0.43	2.60	0.00	4.98	0.75	2.84	0.15	6.47

Table 5. Results of the correlation ( $r$  – correlation coefficient) between the best NDS, SR and SD-type indices and dry phytomass, nitrogen and water content for the  $\alpha$ ,  $GPP_{max}$ , midday GPP, midday  $\varepsilon$  and midday NEE for Amplero, Neustift, Monte Bondone and all sites pooled. The selected bands to compute NSD-, SR- and SD-type indices are reported in brackets. Statistical significance is indicated as \* ( $p < 0.05$ ), \*\* ( $p < 0.01$ ), and \*\*\* ( $p < 0.001$ ).

Index	Site	Parameter	$\alpha$		GPPmax		GPP		$\varepsilon$		NEE		
			Band center [i,j] (nm)	r (-)	Band center [i,j] (nm)	r (-)	Band center [i,j] (nm)	r (-)	Band center [i,j] (nm)	r (-)	Band center [i,j] (nm)	r (-)	
NSD-type	Amplero	Dry phytomass (g m-2)	[900, 910]	-0.81**	[844, 854]	-0.85**	[920, 982]	-0.76*	[462, 466]	-0.87**	[534, 540]	0.60	
	Amplero	Nitrogen content (%)		0.54		0.57		0.44		0.70*		-0.39	
	Amplero	Water content (%)		0.53		0.73*		0.75*		0.66		-0.74*	
	Neustift	Dry phytomass (g m-2)	[972, 998]	-0.04	[908, 930]	0.51	[892, 930]	0.59	[746, 748]	-0.66*	[862, 876]	0.15	
	Neustift	Nitrogen content (%)		0.40		-0.39		-0.46		0.88**		0.18	
	Neustift	Water content (%)		-0.07		0.03		-0.18		0.77*		0.31	
	Monte Bondone	Dry phytomass (g m-2)	[762, 768]	-0.13	[574, 994]	-0.77***	[710, 996]	-0.70***	[402, 762]	-0.74***	[710, 996]	-0.70***	
	Monte Bondone	Nitrogen content (%)		0.29		0.72***		0.62**		0.69***		0.62**	
	Monte Bondone	Water content (%)		0.31		0.69***		0.59**		0.65***		0.59**	
	All	Dry phytomass (g m-2)	[402, 676]	0.23	[736, 976]	0.12	[738, 976]	0.14	[400, 762]	-0.22	[790, 800]	0.06	
	All	Nitrogen content (%)		0.51***		0.19		0.13		0.64***		0.30	
	All	Water content (%)		0.03		-0.09		-0.09		0.32*		0.05	
	SR-type	Amplero	Dry phytomass (g m-2)	[900, 910]	-0.81**	[844, 854]	-0.85**	[982, 920]	-0.76*	[462, 466]	-0.87*	[540, 534]	-0.60
		Amplero	Nitrogen content (%)		0.54		0.57		-0.44		0.70*		0.39
		Amplero	Water content (%)		0.53		0.73*		-0.75*		0.66		0.74*
Neustift		Dry phytomass (g m-2)	[972, 998]	-0.04	[930, 908]	-0.51	[892, 930]	0.59	[746, 478]	-0.66*	[862, 876]	0.15	
Neustift		Nitrogen content (%)		0.40		0.39		-0.46		0.88**		0.18	
Neustift		Water content (%)		-0.07		-0.03		-0.18		0.77*		0.31	
Monte Bondone		Dry phytomass (g m-2)	[768, 762]	0.13	[990, 604]	0.71***	[996, 710]	0.71***	[402, 762]	-0.74***	[996, 700]	0.67*	
Monte Bondone		Nitrogen content (%)		-0.29		-0.69***		-0.62**		0.69***		-0.59	
Monte Bondone		Water content (%)		-0.31		-0.66***		-0.58**		0.64***		-0.55*	
All		Dry phytomass (g m-2)	[402, 676]	0.28	[976, 736]	-0.10	[976, 738]	-0.12	[400, 762]	-0.22	[790, 800]	0.06	
All		Nitrogen content (%)		0.51***		-0.18		-0.13		0.63***		0.30	
All		Water content (%)		-0.01		0.08		0.08		0.33*		0.05	
SD-type		Amplero	Dry phytomass (g m-2)	[900, 910]	-0.80***	[844, 866]	-0.90**	[920, 982]	-0.77*	[492, 496]	-0.76*	[422, 432]	-0.50
		Amplero	Nitrogen content (%)		0.47		0.55		0.46		0.55		0.19
		Amplero	Water content (%)		0.41		0.67*		0.77*		0.43		0.70*
	Neustift	Dry phytomass (g m-2)	[474, 494]	-0.45	[736, 968]	0.20	[878, 922]	0.61	[732, 942]	-0.45	[402, 456]	-0.04	
	Neustift	Nitrogen content (%)		0.33		0.09		-0.34		0.90**		-0.28	
	Neustift	Water content (%)		0.15		0.51		-0.04		0.80*		-0.72*	
	Monte Bondone	Dry phytomass (g m-2)	[762, 768]	-0.38	[444, 482]	0.65***	[436, 488]	0.60**	[658, 682]	0.67***	[450, 486]	0.60**	
	Monte Bondone	Nitrogen content (%)		0.53***		-0.58**		-0.58**		-0.62**		-0.59**	
	Monte Bondone	Water content (%)		0.52***		-0.58**		-0.58		-0.56**		-0.55**	
	All	Dry phytomass (g m-2)	[822, 824]	0.45***	[550, 560]	0.12	[414, 470]	0.00	[732, 928]	0.55***	[468, 660]	-0.11	
	All	Nitrogen content (%)		-0.09		-0.09		-0.15		0.16		-0.33*	
	All	Water content (%)		-0.08		0.18		0.19		-0.53***		0.24	

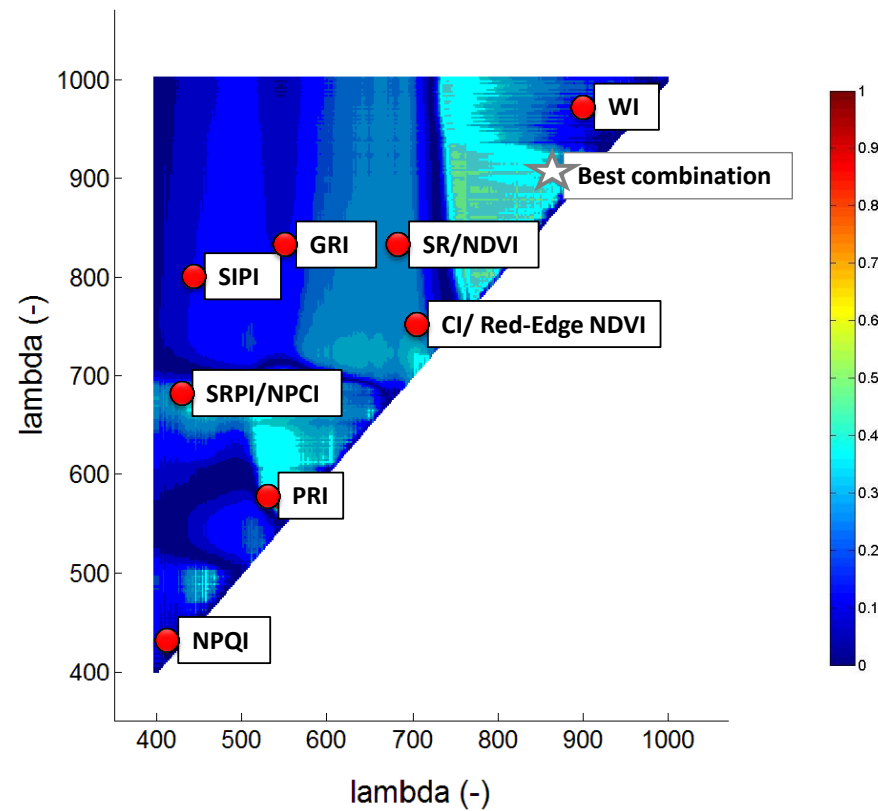


Figure 1. A selected example of a correlogram between NSD-type indices and midday average GPP for all sites pooled. The correlogram shows all  $R^2$  values, the asterisk symbol indicates the two-band combination with the highest  $R^2$  value and the dots indicate the location of the reference VIs reported in Table 2 (SR: Simple ratio; GRI: Green Ratio Index; WI: Water Index; SRPI: Simple Ratio Pigment Index; NDVI: Normalized Difference Vegetation Index; NPQ: Normalized Phaeophytinization Index; NPCI: Normalized Pigment Chlorophyll Index; CI: Chlorophyll Index; Red Edge NDVI; SIPI: Structural Independent Pigment Index; PRI: Photochemical Reflectance Index).

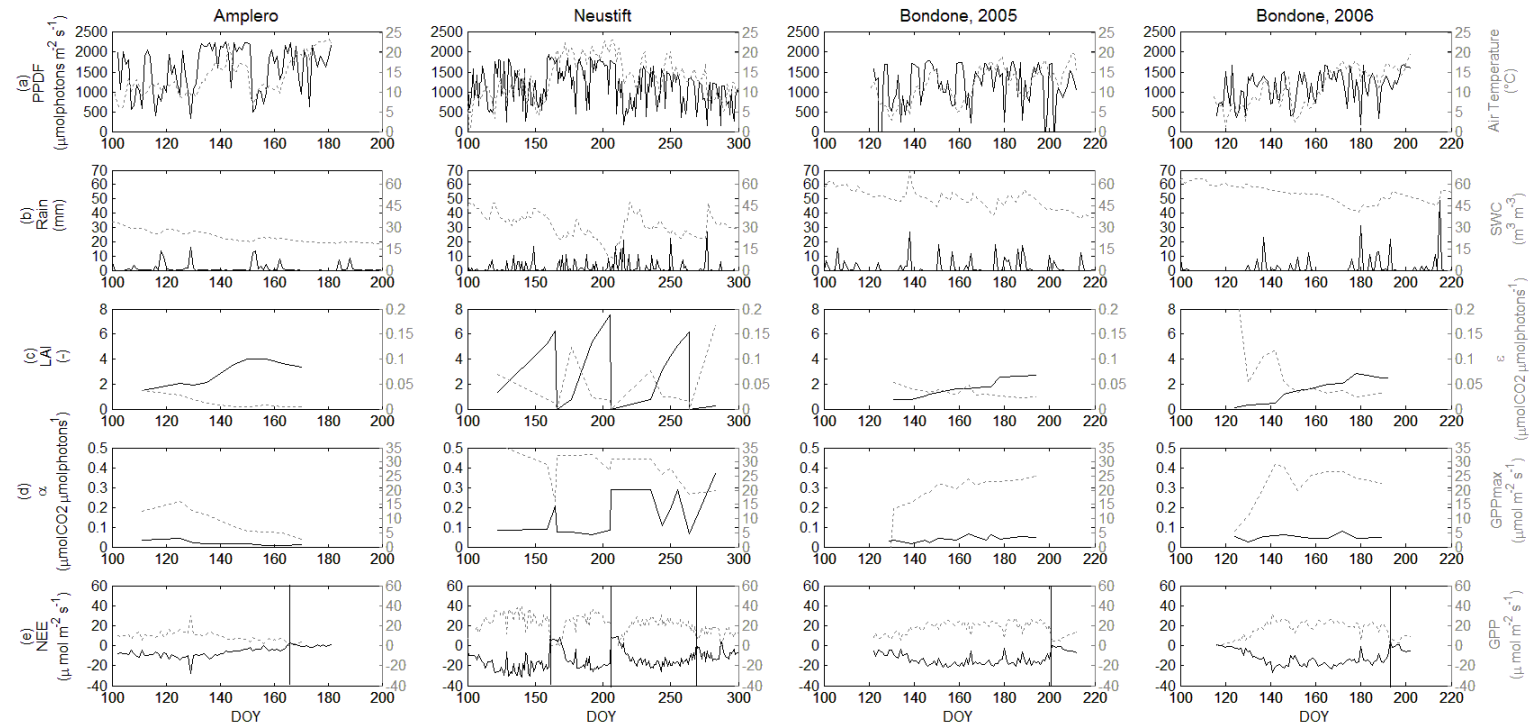


Figure 2. Seasonal variation of meteorological variables, LAI, CO<sub>2</sub> fluxes and ecophysiological parameters for the period of the hyperspectral measurements at the three investigated grasslands. (a) midday average photosynthetically active radiation (PAR;  $\mu\text{mol m}^{-2} \text{s}^{-1}$ ; solid black line) and daily average air temperature ( $^{\circ}\text{C}$ ; dotted grey line); (b) daily precipitation (Rain; mm; solid black line) and daily average soil water content (SWC;  $\text{m}^3 \text{m}^{-3}$ ; dotted grey line); (c) Leaf Area Index (LAI;  $\text{m}^2 \text{m}^{-2}$ ; solid black line) and light use efficiency ( $\epsilon$ ;  $\mu\text{mol photons } \mu\text{mol CO}_2^{-1}$ ; dotted grey line); (d) apparent quantum yield ( $\alpha$ ;  $\mu\text{mol CO}_2 \mu\text{mol photons}^{-1}$ ; solid black line) and gross primary production at saturating light ( $\text{GPP}_{\text{max}}$ ;  $\mu\text{mol m}^{-2} \text{s}^{-1}$ ; dotted grey line); (e) midday average net ecosystem CO<sub>2</sub> exchange (NEE;  $\mu\text{mol m}^{-2} \text{s}^{-1}$ ; solid black line) and gross primary production (GPP;  $\mu\text{mol m}^{-2} \text{s}^{-1}$ ; grey dotted line); vertical lines in the lowermost panels indicate the dates of mowing.

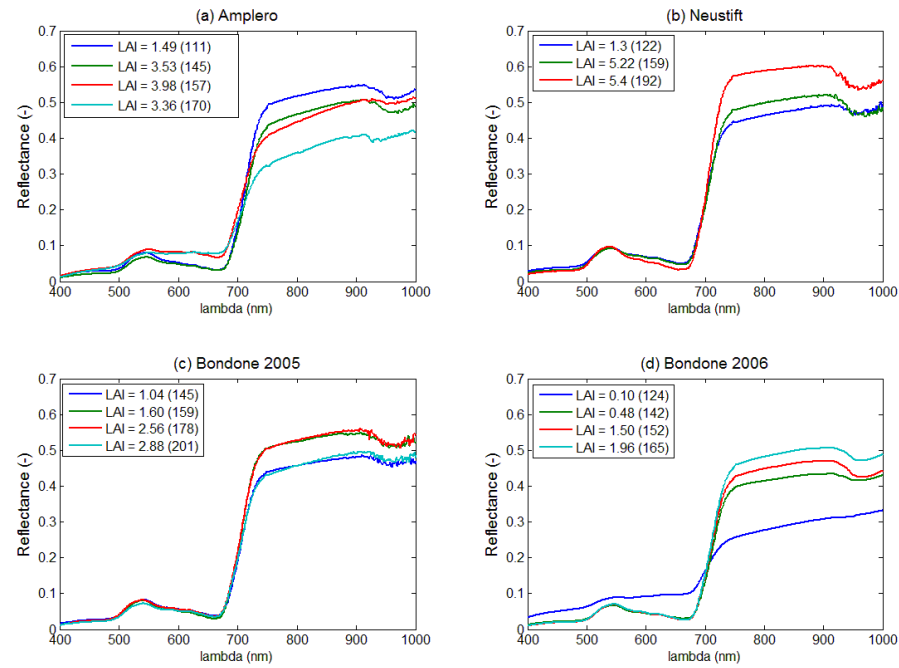


Figure 3. Selected grassland spectral signatures during the growing seasons. The figure legends indicates the corresponding leaf area index (LAI;  $m^2 m^{-2}$ ) and the day of year (in parenthesis).

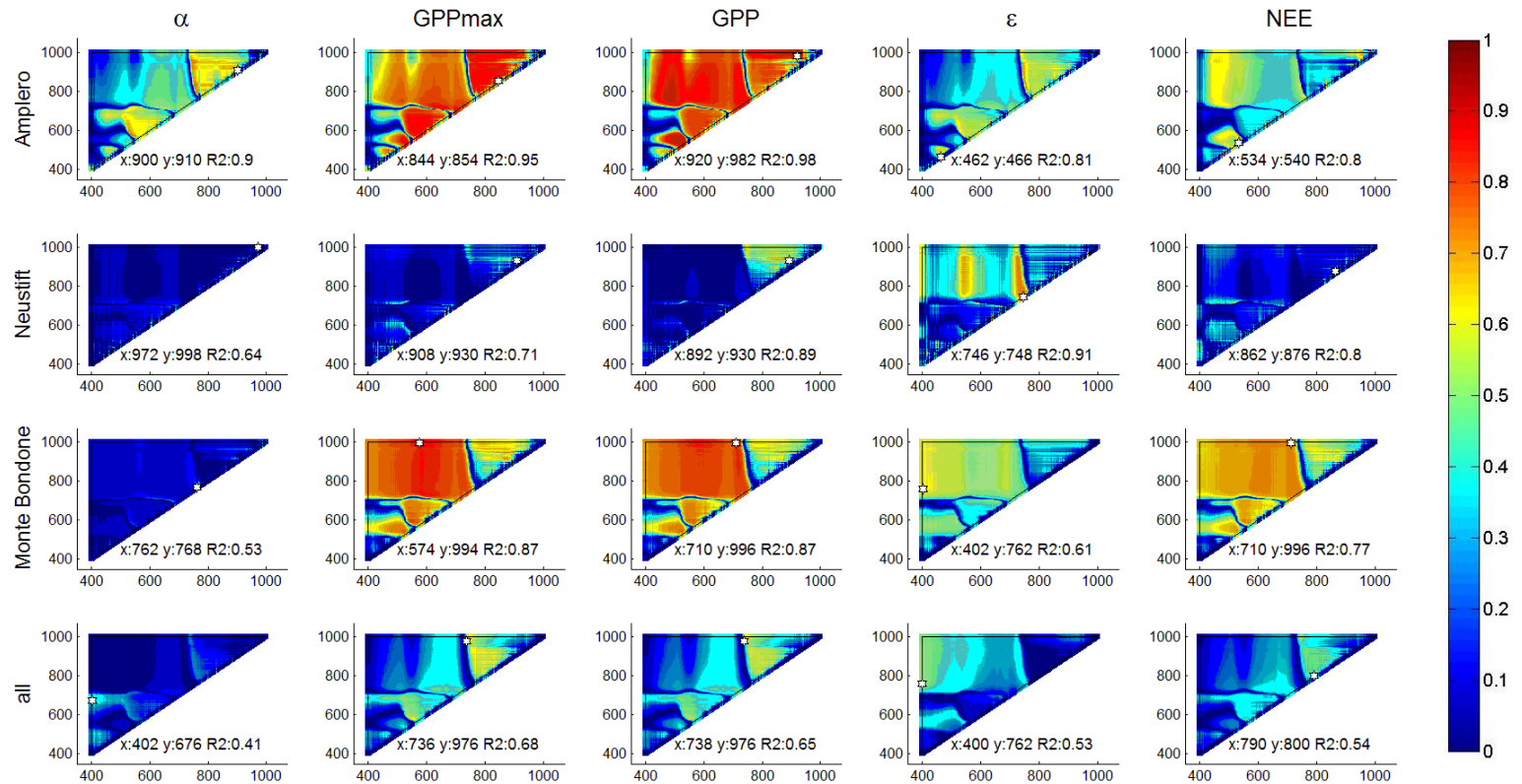


Figure 4. Correlograms of  $R^2$  values for  $\alpha$ ,  $GPP_{max}$  and midday averaged GPP,  $\epsilon$  and NEE and NSD-type indices for Amplero, Neustift, Monte Bondone (both study years pooled) and all sites pooled. The asterisks indicate the position of paired band combinations corresponding to the maximum  $R^2$ .



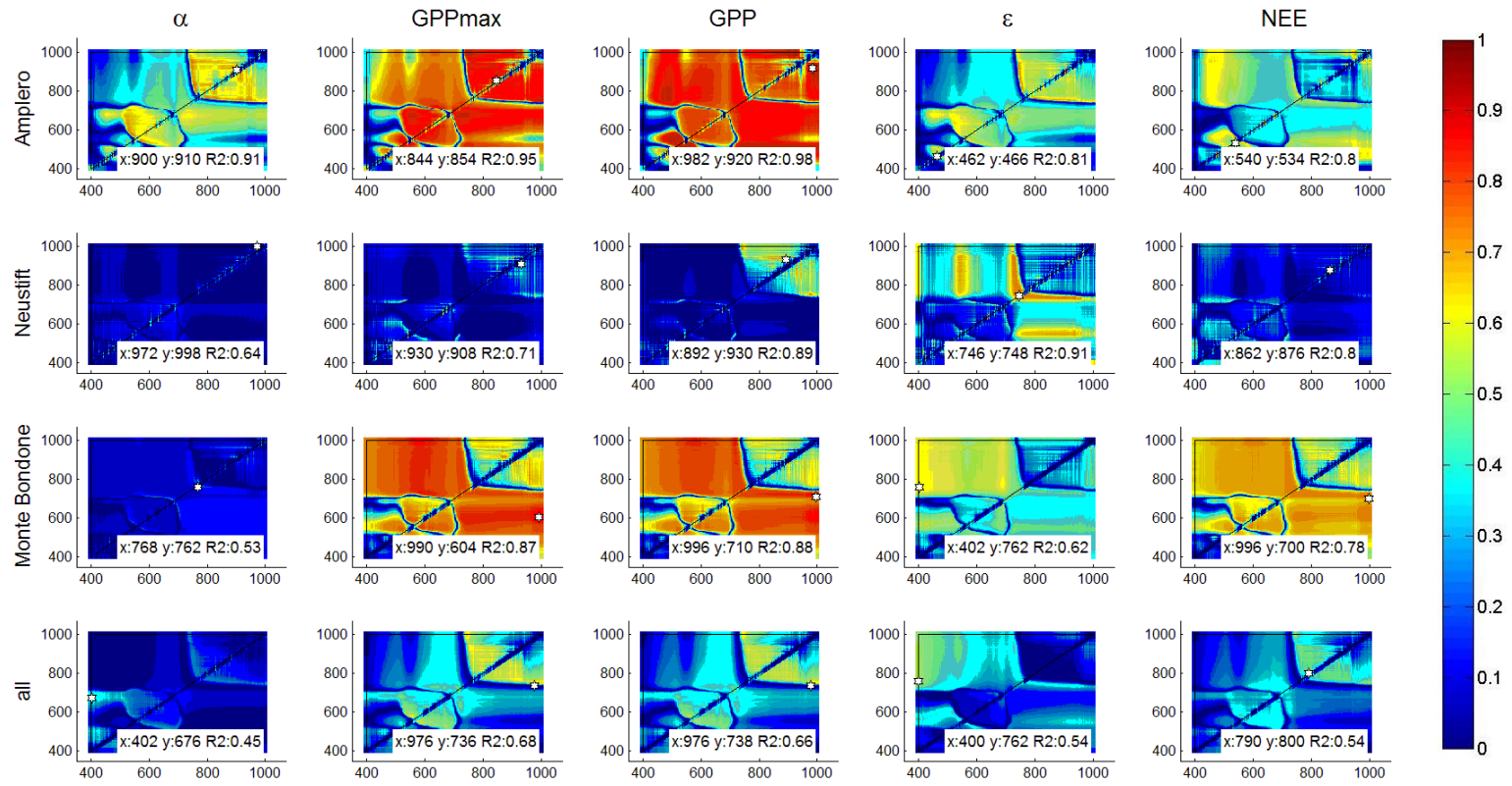


Figure 5. Correlograms of  $R^2$  values for  $\alpha$ ,  $GPP_{max}$  and midday averaged GPP,  $\epsilon$  and NEE and SR-type indices for Amplero, Neustift, Monte Bondone (both study years pooled) and all sites pooled. The asterisks indicate the position of paired band combinations corresponding to the maximum  $R^2$ .

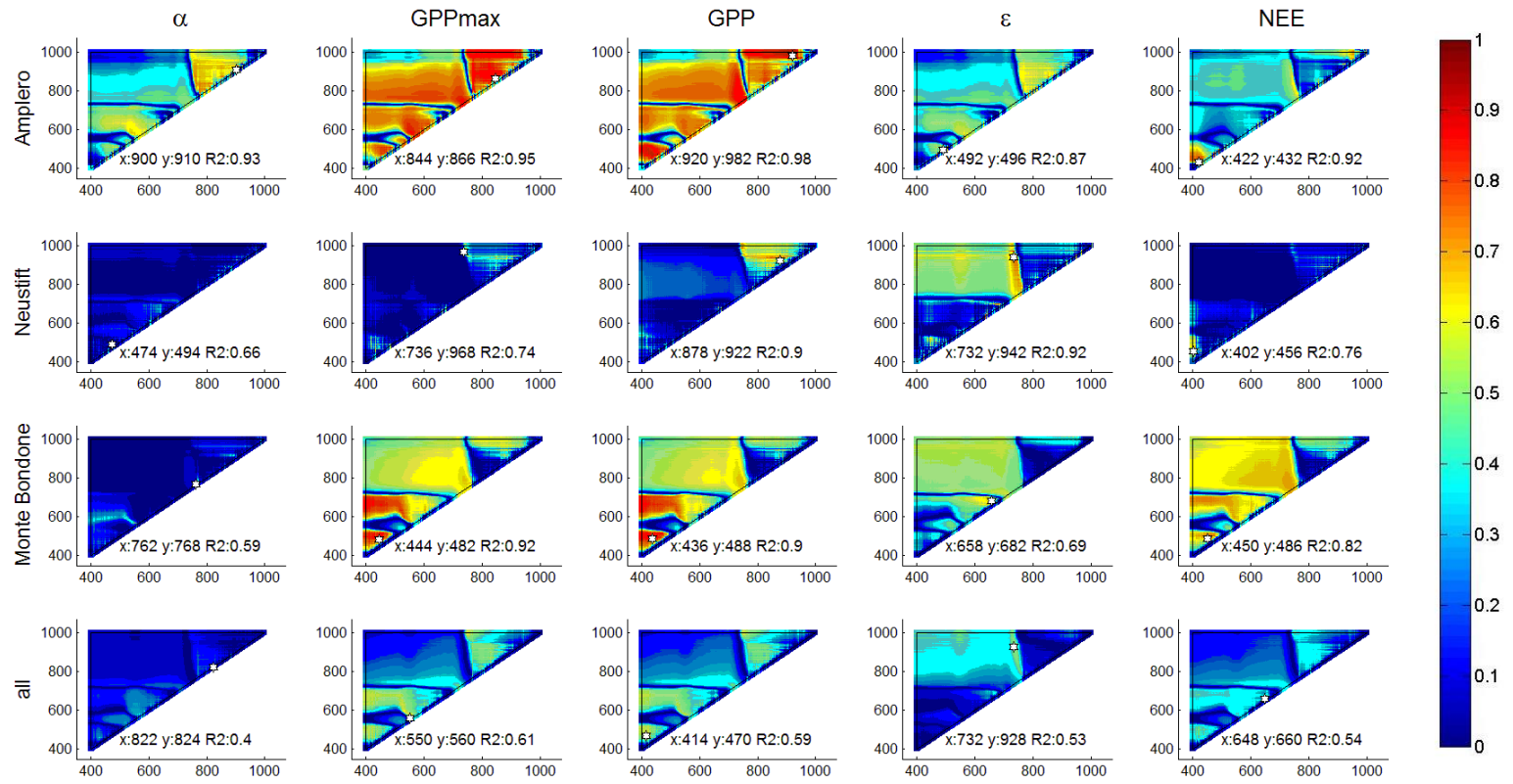


Figure 6. Correlograms of  $R^2$  values for  $\alpha$ ,  $GPP_{max}$  and midday averaged GPP,  $\epsilon$  and NEE and SD-type indices for Amplero, Neustift, Monte Bondone (both study years pooled) and all sites pooled. The asterisks indicate the position of paired band combinations corresponding to the maximum  $R^2$ .

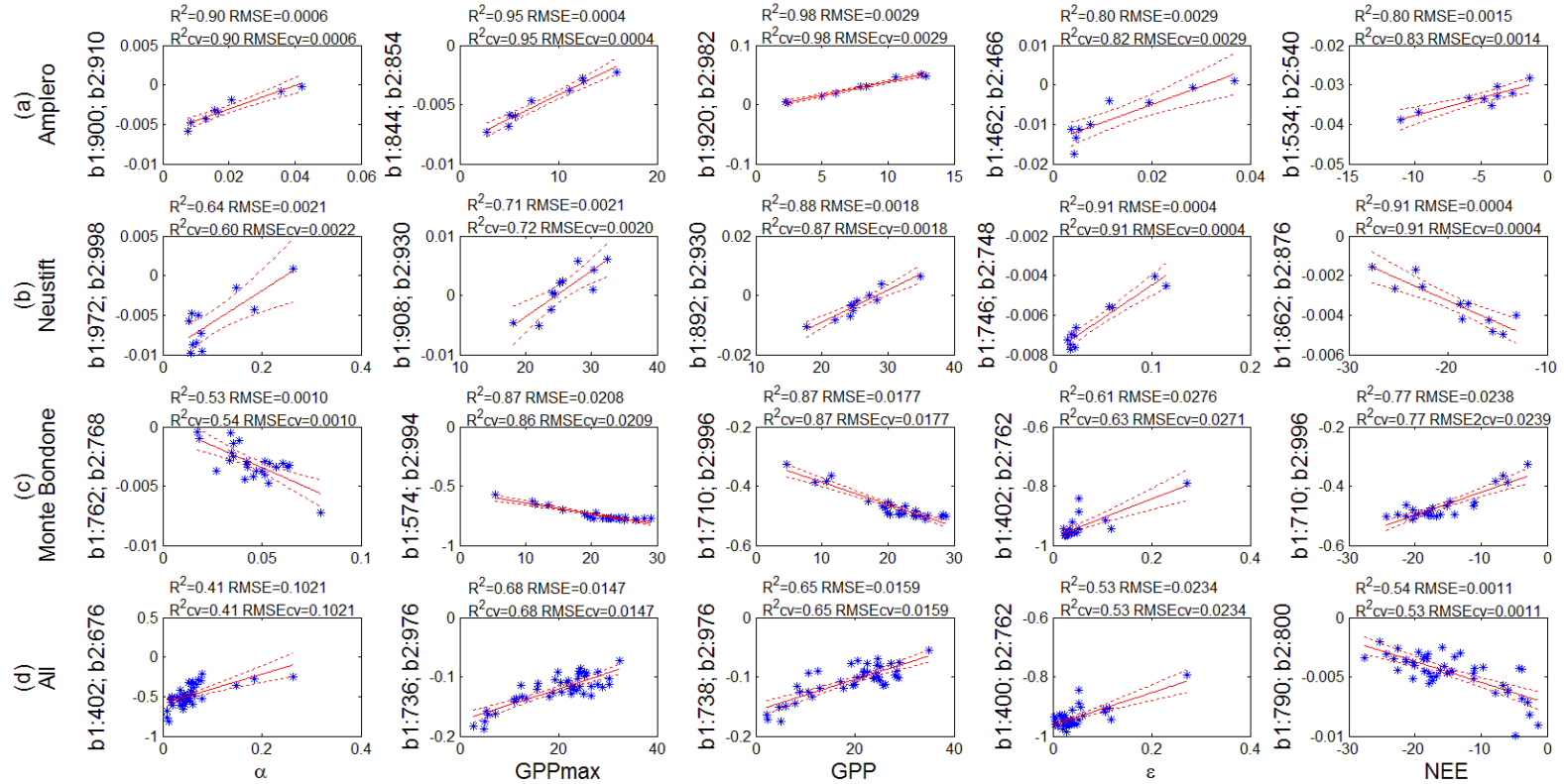


Figure 7. Results of linear correlation analysis for  $\alpha$ ,  $GPP_{max}$  and midday averaged  $GPP$ ,  $\epsilon$  and  $NEE$  and selected best NSD-type indices for (a) Amplero, (b) Neustift, (c) Monte Bondone (both study years pooled) and (d) all sites pooled.  $R^2$ —Coefficient of determination;  $RMSE$ —Root Mean Square Error;  $R^2_{cv}$ —Cross-validated coefficient of determination;  $RMSE_{cv}$ — Cross-validated root Mean Square Error. The solid red lines indicate the fitted models and the dotted red lines represent the 95% upper and lower confidence bounds.

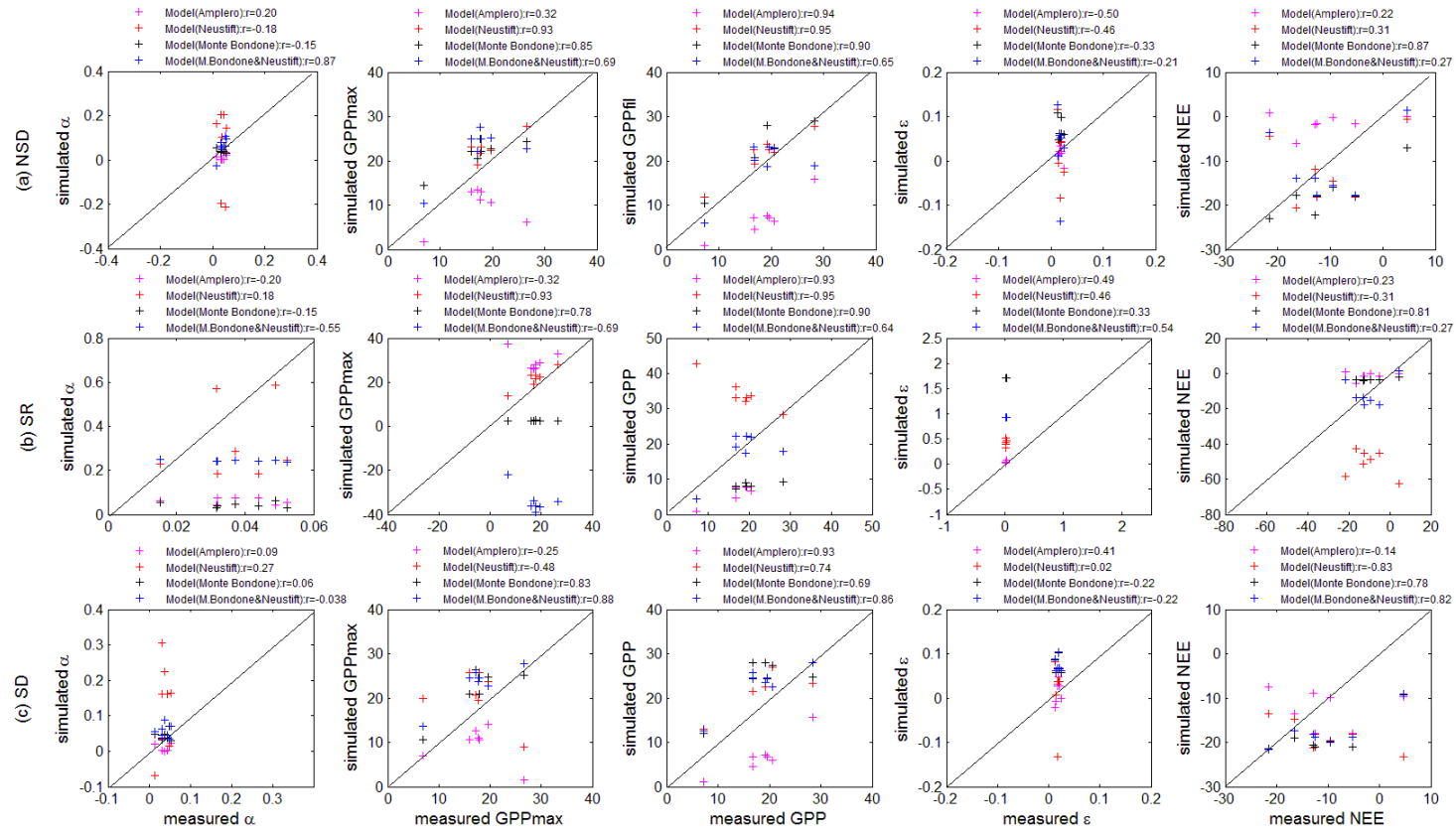


Figure 8. Results of validation of linear regression models between VIs ((a) NSD-type; (b) SR-type; (c) SD-type) and ecophysiological parameters:  $\alpha$ ,  $\epsilon$  (midday average),  $GPP_{max}$  and midday average  $CO_2$  fluxes (NEE and GPP).  $r$ —coefficient of correlation. Different colours represent results of the validation performed applying to the three new sites the model for Amplero (in magenta), Neustift (in red) and Monte Bondone (in blue) and a model parameterized grouping Neustift and Monte Bondone (in black).

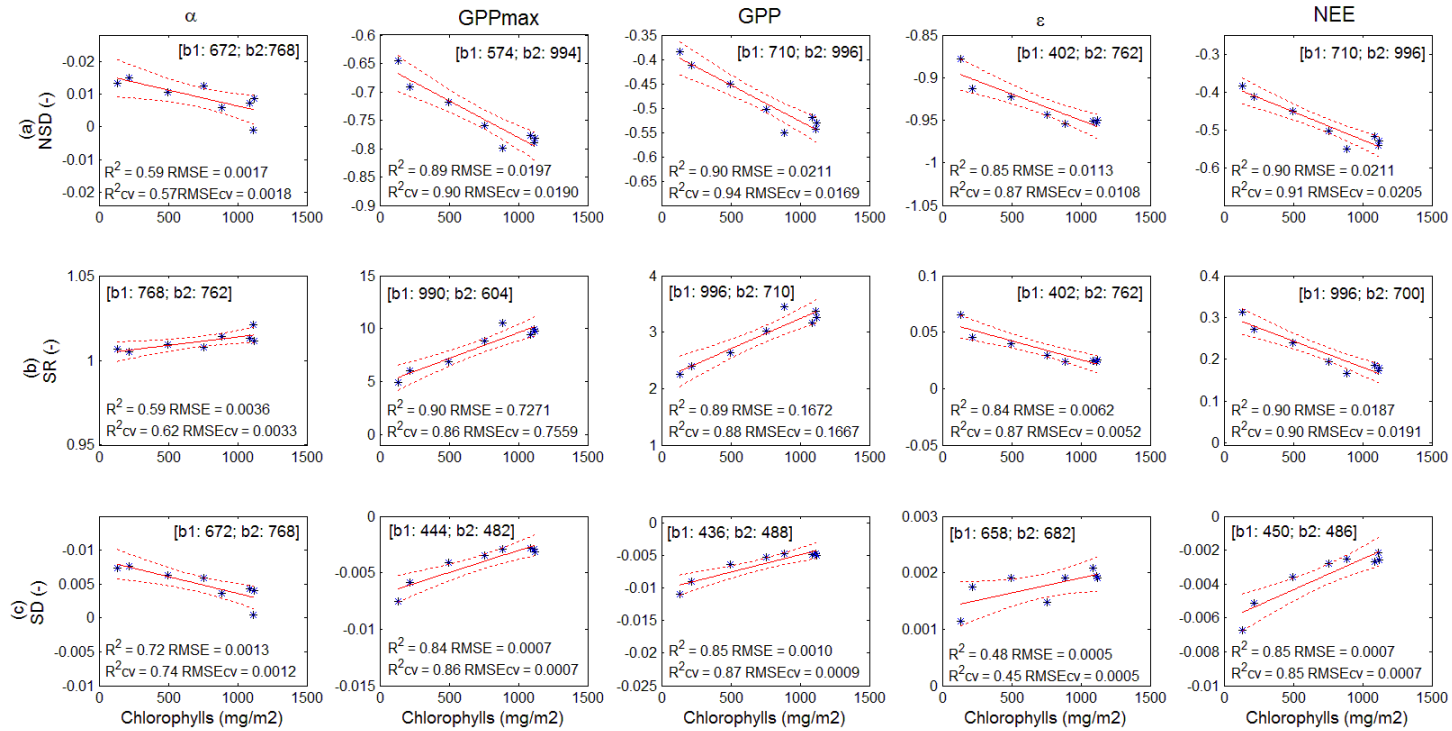
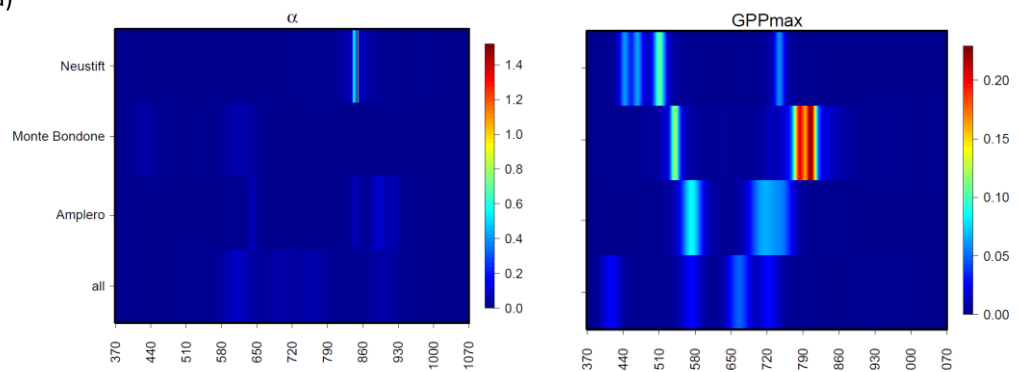
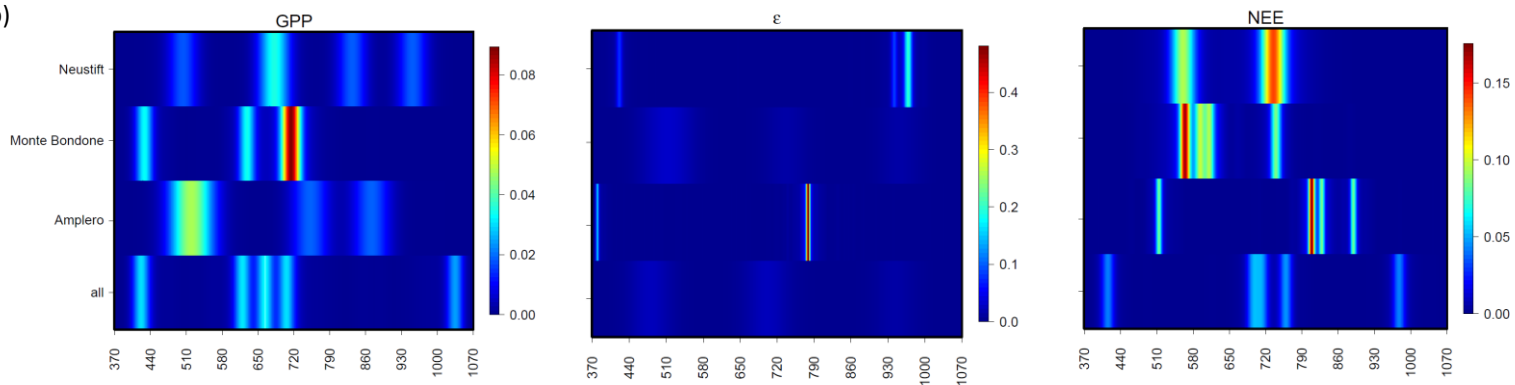


Figure 9. Correlation between selected (a) NSD-, (b) SR- and (c) SD-type indices and the total chlorophyll content for  $\alpha$ ,  $\epsilon$  (midday average),  $GPP_{max}$  and midday average CO<sub>2</sub> fluxes (NEE and GPP) for Monte Bondone in 2013.  $R^2$ — coefficient of correlation; RMSE—root mean square error;  $R^2_{cv}$ — cross-validated coefficient of correlation; RMSE<sub>cv</sub>— cross-validated root mean square error. The solid red lines indicate the fitted models and the dotted red lines represent the 95% upper and lower confidence bounds. The selected bands to compute NSD-, SR- and SD-type indices are reported in brackets.

(a)



(b)



(c)

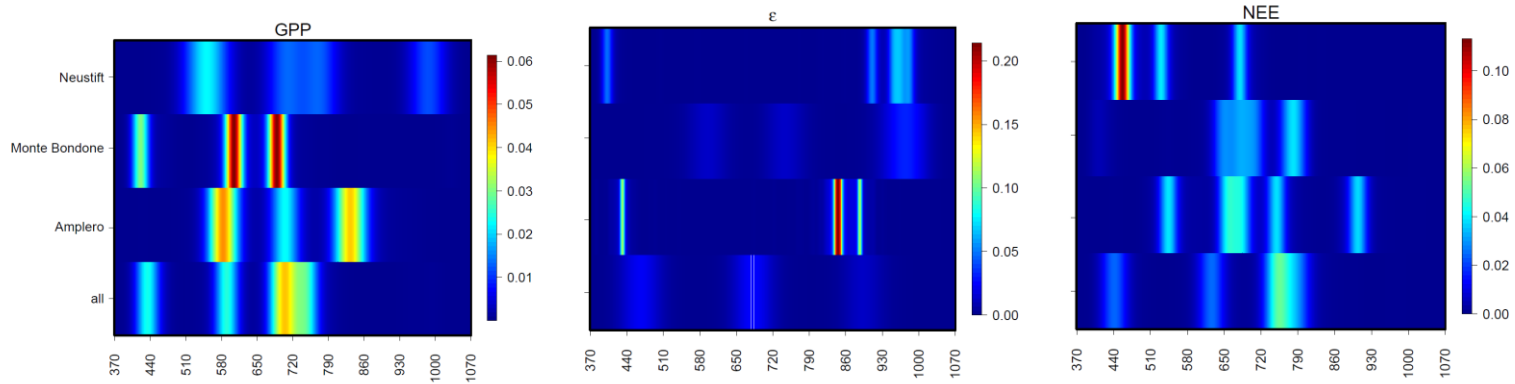


Figure 10. Results of the GA-rF method for band selection for Amplero, Neustift, Monte Bondone and all sites pooled for (a)  $\alpha$  and  $GPP_{max}$ , (b) midday average  $\varepsilon$ ,  $CO_2$  fluxes (NEE and GPP); (b) daily average  $\varepsilon$  and  $CO_2$  fluxes (NEE and GPP).

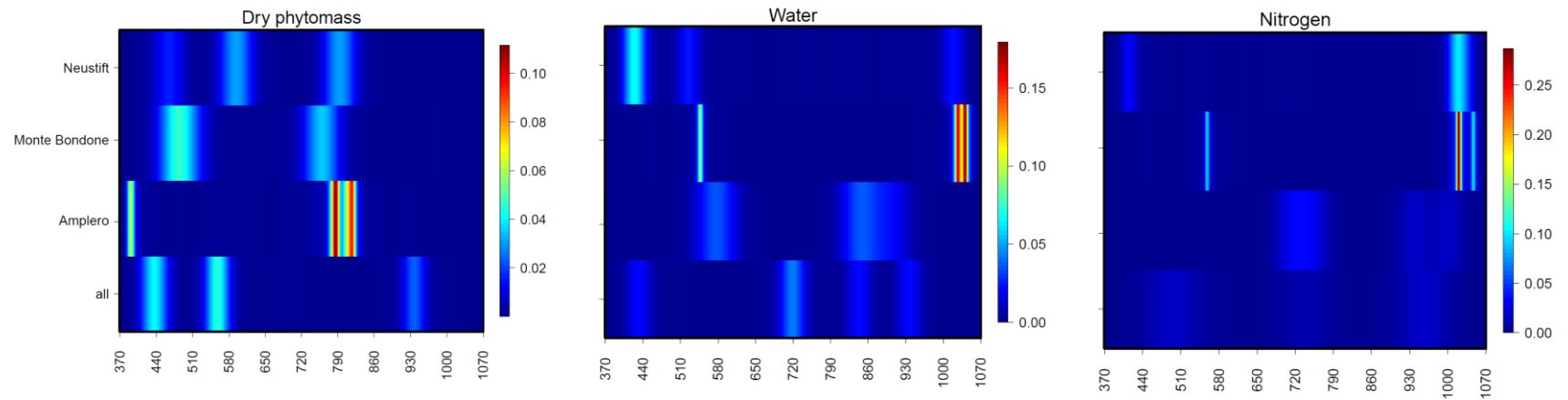


Figure 11. Results of the GA-rF method for band selection for Amplero, Neustift, Monte Bondone and all sites pooled for dry phytomass, water and nitrogen content.